Sub-seasonal Prediction of Central European Summer Heatwaves with Linear and Random Forest Machine Learning Models

Elizabeth Weirich Benet,[a] Maria Pyrina,[a] Bernat Jiménez Esteve,[a] Ernest Fraenkel,[b] Judah Cohen,[c,d] and Daniela I.V. Domeisen[a,e]

[a] *Institute for Atmospheric and Climate Science, ETH Zürich, Zürich, Switzerland*

[b] *Department of Biological Engineering, MIT, Cambridge, USA*

[c] *Atmospheric and Environmental Research (AER), Lexington, USA*

[d] *Department of Civil and Environmental Engineering, MIT, Cambridge, USA*

[e] *Institute of Earth Surface Dynamics, Université de Lausanne, Lausanne, Switzerland*

Corresponding author: Elizabeth Weirich Benet (weiriche@ethz.ch) and Daniela I.V. Domeisen (daniela.domeisen@env.ethz.ch)

ABSTRACT: Heatwaves are extreme near-surface temperature events that can have substantial impacts on ecosystems and society. Early Warning Systems help to reduce these impacts. However, state-of-the-art prediction systems can often not make accurate forecasts of heatwaves more than two weeks in advance, which are required for advance warnings. We therefore investigate the potential of statistical and machine learning methods to understand and predict central European summer heatwaves on time scales of several weeks. As a first step, we identify the most important atmospheric and surface predictors based on previous studies and supported by a correlation analysis: 2-m air temperature, 500-hPa geopotential, precipitation, and soil moisture in central Europe, as well as Mediterranean and North Atlantic sea surface temperatures, and the North Atlantic jet stream. Based on these predictors, we apply machine learning methods to forecast summer temperature anomalies and the probability of heatwaves for 1–6 weeks lead time at weekly resolution. For each of these two target variables, we use both a linear and a Random Forest model. The performance of these models decays with lead time, as expected, but outperforms persistence and climatology at all lead times. For lead times longer than two weeks, our machine learning models beat the European Centre for Medium-Range Weather prediction system. We thus show that machine learning can help extend the forecasting lead time of summer temperature anomalies and heatwaves.

SIGNIFICANCE STATEMENT: Heatwaves (prolonged extremely warm temperatures) cause thousands of fatalities worldwide each year. These damaging events are becoming even more severe with climate change. This study aims to improve advance predictions of summer heatwaves in central Europe by using statistical and machine learning methods. Machine learning models are shown to outperform conventional physics-based models for forecasting heatwaves more than two weeks in advance. These early warnings can be used to activate effective and timely response plans targeting vulnerable communities and regions, thereby reducing the damage caused by heatwaves.

1. Introduction

A heatwave is an extended period of extremely hot weather relative to the expected local conditions at that time of the year. These high temperatures can cause substantial damage to human health, agriculture, infrastructure, and biodiversity (Perkins 2015; Barriopedro et al. 2011). However, although heatwaves are among the most dangerous natural hazards, their corresponding death and destruction tolls are not always immediately obvious (Wallemacq et al. 2018; Basu 2002; Lowe et al. 2011), making heatwaves *silent killers* (Loughnan 2014). Between 1998 and 2017, globally more than 166’000 people died due to heatwaves – the 2003 European heatwave alone caused 70’000 deaths (Wallemacq et al. 2018). In addition, the probability of other natural disasters, such as wildfires, is higher during heatwaves (e.g., the Australian wildfires 2020 ignited amid a record-breaking heatwave (Deb et al. 2020)). Furthermore, the variability of global temperature is increasing with climate change. Combined with global warming, this trend results in more extreme hot weather (Perkins 2015; Barriopedro et al. 2011). As a consequence of climate change, heatwaves are increasing in intensity, duration, and frequency (Ford et al. 2018; Perkins and Alexander 2013; Perkins-Kirkpatrick and Lewis 2020; Seneviratne et al. 2014).

Early warning systems (EWS) are one of the most effective climate adaptation measures (WMO 2021), because they enable effective and timely response plans that target vulnerable populations and regions. For instance, EWSs help to determine when crops will need more irrigation or when local hospitals must prepare for an additional number of patients (Bassil and Cole 2010). However, the time needed to prepare for heatwaves is often beyond the time scales of medium-range weather forecasts (up to two weeks) that are currently available (de Perez et al. 2018). While long-term averages on seasonal time scales show some predictability, a gap of forecast skill between two weeks and seasonal scales remains (White et al. 2017; Robertson et al. 2015). Alternative approaches must therefore be explored to extend the lead time of skillful forecasts to sub-seasonal time scales (two weeks to two months).

A variety of machine learning (ML) and deep learning (DL) models have been used for extreme weather forecasting (Reichstein et al. 2019; Cho et al. 2020; Khan et al. 2019; Kretschmer et al. 2017; Lehmann et al. 2020; Liu et al. 2016; Racah et al. 2016; Chattopadhyay et al. 2020). Other studies have focused on ML-based summer temperature and heatwave forecasting (Kämäräinen et al. 2019; Pyrina et al. 2021; Vijverberg et al. 2020; Sobhani et al. 2018). However, these studies target either seasonal instead of sub-seasonal scales (Kämäräinen et al. 2019; Pyrina et al. 2021), North America instead of central Europe (CE) (Vijverberg et al. 2020; Sobhani et al. 2018), or focus on identifying physical drivers of heatwaves and not on a comparison of the model performance to dynamical prediction models (van Straaten et al. 2022). Moreover, summer heatwaves have stronger impacts due to the absolute temperatures they reach, leading to higher mortality rates than in winter (US EPA 2016). This makes summer heatwaves more harmful than winter heatwaves, which are usually associated with milder conditions.

In this study, we investigate central European sub-seasonal forecasting of summer heatwaves using statistical and ML methods. We aim at answering the following research questions:

(i) Which predictors are the most relevant for sub-seasonal forecasts of summer temperature anomalies in CE?

(ii) Can the sub-seasonal forecasting accuracy of summer temperature anomalies and heatwaves in CE be improved by using ML methods based on the predictors identified in (i)?

In order to answer these two questions, we first select a set of atmospheric and surface predictors which, based on previous studies, are thought to have the largest impact on heatwave prediction (Perkins and Alexander 2013; Li et al. 2020; Perkins 2015; Zschenderlein et al. 2020; Suarez-Gutierrez et al. 2020; Oliveira et al. 2020; Bladé et al. 2011; Dong et al. 2013; Ossó et al. 2020; Mecking et al. 2019; Duchez et al. 2016; Black et al. 2004; Fischer et al. 2007; Kolstad et al. 2017; Seneviratne et al. 2010). We consider both remote drivers, which are linked to CE temperatures via teleconnections, and local drivers (see Sec 2). Additionally, we conduct a linear correlation analysis between each potential predictor and 2-m air temperature. We then use these predictors as the input for ML models to forecast summer temperature anomalies and the probability of heatwaves at lead times from one to six weeks. For each of the two forecast problems we use both a linear model and a random forest (RF) model. The methods are presented in Section 3, the results and limitations of our study are discussed in Sections 4 and 5, respectively, and we conclude in Section 6.

We show that ML models can help extend the forecasting lead time of summer temperature anomalies and heatwaves when compared to the European Centre for Medium-Range Weather Forecasts (ECMWF) prediction system. These improved forecasts can be used to enhance EWS.

2. Physics of heatwaves

Summer heatwaves differ from winter heatwaves, as they are driven by different mechanisms: while winter European heatwaves are mainly driven by warm air advection from the equator, summer European heatwaves are based on persistent high-pressure systems (blocking highs) (Perkins and Alexander 2013; Li et al. 2020; Perkins 2015; Zschenderlein et al. 2020). We therefore expect forecasting models that are trained separately for summer and winter to perform better and focus exclusively on drivers of summer heatwaves.

By reviewing the physical mechanisms behind central European summer heatwaves, we identify a set of relevant predictors. First, the local geopotential associated with blocking anticyclones and upper level ridges can drive summer heatwaves on short time scales (up to a couple of weeks) (Suarez-Gutierrez et al. 2020; Kautz et al. 2022). Hereby, the geopotential at the 500-hPa pressure level is typically used to avoid capturing the bidirectional influence between surface temperature and surface pressure (i.e., the high temperature leading to low pressure near the ground) (Suarez-Gutierrez et al. 2020). Second, leading modes of large-scale atmospheric variability relevant for summer European climate are found to be linked to the latitude and speed of the North Atlantic (NA) jet stream (Oliveira et al. 2020). The occurrence and persistence of weather regimes can be used to characterise the location and intensity of the NA storm track, thus acting as key predictors for near-surface temperature extremes over Europe (Bladé et al. 2011; Dong et al. 2013). In particular, the Summer East Atlantic (SEA) pattern (i.e., the second dominant mode of summer low-frequency variability in the Euro-Atlantic region) can significantly influence temperatures and precipitation over Europe during summer months Wulff et al. (2017).

Third, cold sea surface temperature (SST) anomalies in the NA are found to be present prior to the onset of the most extreme European heat waves since 1980 (Duchez et al. 2016). For instance, anomalously cold SSTs in the NA were key to the development of the 2015 European heatwave (Mecking et al. 2019). Moreover, northwestern Mediterranean (NWMED) SSTs are linked to temperatures over the European continent due to their proximity and large heat capacity, acting as a heat buffer for land temperatures (e.g., the 2003 European heatwave was connected to warm Mediterranean SSTs) (Black et al. 2004).

Furthermore, precipitation is associated with low pressure systems (cyclones). During a cyclone, clouds reduce the amount of solar radiation reaching the surface, which results in less sensible heat flux and a lower surface air temperature. Finally, precipitation directly influences soil moisture, which is a further driver of summer heatwaves (Fischer et al. 2007). A drying pattern (low soil moisture) and warming reinforce each other due to a positive feedback effect (Kolstad et al. 2017): If soil is moist, the incoming solar radiation is used more towards latent heat flux to the atmosphere, whereas, if soil is dry, it emits more sensible heat. For this reason, drier soil will heat up faster than moist soil. This will, in turn, result in less soil moisture and thus, in even more dryness, closing the positive feedback loop (Seneviratne et al. 2010); if the preceding winter and spring have been dry, extremely high summertime temperatures are more likely to occur over Europe (Perkins 2015).

3. Methods

a. Heatwave index definitions

We define weekly heatwaves via a binary index: one for a heatwave week and zero, otherwise. While there is no universal definition for heatwaves and a range of different indices are found across the literature, percentile-based definitions are widely used (Perkins 2015; Perkins and Alexander 2013; Perkins-Kirkpatrick and Lewis 2020; Spensberger et al. 2020). We use two different heatwave definitions: $+1\sigma$ for high and $+1.5\sigma$ for extremely high temperature anomalies (see Fig 1). The $+1\sigma$ weekly heatwave index is defined as one for the weekly mean temperature anomalies above one standard deviation (σ) (i.e., to the right of the orange line in Figure 1) and zero, otherwise. Analogously, the $+1.5\sigma$ weekly heatwave index is defined as one for the weekly mean temperature anomalies above 1.5 standard deviations (i.e., to the right of the red line in Figure 1) and zero, otherwise.

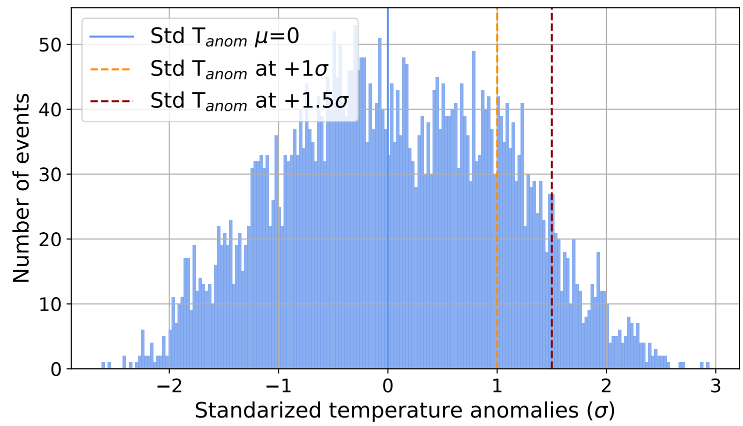

FIG. 1: **Histogram of temperature anomalies for the definition of heatwave indices** The blue bars correspond to the standardized ($\mu = 0$, $\sigma = 1$) temperature anomalies. The data is smoothed by a 7-day running mean (see Sec 3b2). The vertical blue line marks the mean ($\mu = 0$) of the distribution. The stippled orange (red) line marks +1 (+1.5) standard deviations (σ) from the mean and is used to define heatwaves.

b. Data

1) PREDICTORS

We select seven atmospheric and surface predictors that we expect to be related to summer temperature and heatwaves in CE based on previous studies (see Sec 2) and a correlation analysis (see Sec 4b1). These predictors are: 2-m air *temperature*, 500-hPa *geopotential*, *precipitation*, *soil moisture*, the *SEA* index, *NWMED SST*, and *cold North Atlantic anomaly (CNAA) SST*. This set of predictors is considered in the extended summer season (MJJAS), during the time period between 1 May 1981 and 30 September 2018. Further technical details about these predictors can be found in Table 1. Since both local predictors and remote teleconnections are included, location details are shown in Figure 2 and their latitude-longitude coordinates are provided in Table 2. Moreover, to assess the robustness of our models, the analysis is repeated on 110 years of ERA20C data (1900–2009). The results are similar and are not shown here.

(i) Calculation of the SEA index The changes in speed and location of the NA jet stream are included in our set of predictors through the *SEA* index. First, the *SEA* pattern is calculated via principal component analysis (PCA) (Storch and Zwiers 2003), applied on the detrended 500-hPa geopotential height anomalies over the NA box for the summer season (JJA). The *SEA* index corresponds to the time dependent coefficients (or PCA amplitudes) of the second PCA pattern

(Wulff et al. 2017). Then, the daily *SEA* index is calculated for the extended summer season (MJJAS) by projecting the *SEA* pattern on the daily values of the 500-hPa geopotential height anomalies from May to September. After the index is calculated, the obtained time series are normalised to a mean equal to zero and standard deviation equal to one.

Predictor	**Physical magnitude (units)**	**Source (Space, Time Res.)**	**Level**	**Box**	**Method**
Temperature	2-m air temperature (^{o}C)	E-OBS (0.25^{o}, daily)	2 m a.g.	CE	avg
Geopotential	geopotential (m^2 s^{-2})	ERA-Interim (2.5^{o}, daily)	500 hPa	CE	avg
Precipitation	thickness of rainfall amount (mm)	E-OBS (0.25^{o}, daily)	surface	CE	avg
Soil moisture	volumetric soil water layer (m^3 m^{-3})	ERA5-Land (2.5^{o}, daily)	0–28 cm u.g.	CE	avg
SEA index	geopotential (m^2 s^{-2})	ERA-Interim (2.5^{o}, daily)	500 hPa	NA	PCA
NWMED SST	sea surface temperature (^{o}C)	HadISST (1^{o}, monthly)	sea level	NWMED	avg
CNAA SST	sea surface temperature (^{o}C)	HadISST (1^{o}, monthly)	sea level	CNAA	avg

TABLE 1: **Properties of the predictors** For each predictor, the name of the corresponding variable (physical magnitude) as labeled in the dataset (source) is presented. We also indicate the temporal and spatial resolution at which each variable was downloaded, the extracted vertical level, the selected spatial location, and the method used to convert the two-dimensional latitude-longitude field into a one-dimensional time series. The soil moisture (0–28 cm u.g.) is calculated as the average over the first two layers (layer one: 0–7 cm u.g. and layer two: 7–28 cm u.g.). The monthly SST predictors are interpolated to daily time resolution. Notation: a.g.: above ground and u.g.: underground.

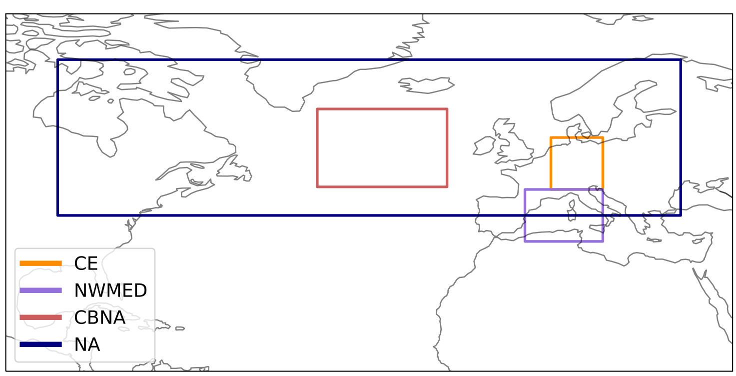

FIG. 2: **Location of latitude-longitude boxes** Used to define the location of the predictors shown in Table 1. The latitude-longitude coordinates of the boxes are shown in Table 2.

2) DATA PREPROCESSING PIPELINE

(1) First, we select latitude-longitude boxes for each physical magnitude and take either the average over the corresponding box or perform a PCA (see Tab 1). By removing the spatial

Box	Latitude	Longitude
Central Europe (CE)	45°N–55°N	5°E–15°E
North Atlantic (NA)	40°N–70°N	90°W–30°E
Northwestern Mediterranean (NWMED)	35°N–45°N	0°–15°E
Cold North Atlantic anomaly (CNAA) (Duchez et al. 2016)	45°N–60°N	15°W–40°W

TABLE 2: **Coordinates of latitude-longitude boxes** The boxes correspond to the location of the predictors of Table 1 as seen in Figure 2.

dimension, we obtain one-dimensional time series. (2) Second, the maximum overlapping time period for the selected predictors is chosen: 1 May 1981 to 30 September 2018 (38 summers). (3) We then detrend each time series by subtracting the linear trend. Detrending the data removes linear long-term trends. (4) Next, we compute the daily climatology (x_{clim}), which is defined as the mean over the full time period for a particular day of the year. We smooth the daily climatology by a centred 31-day rolling mean window. (5) We then compute the anomalies with respect to climatology as: $x_{\text{anom}} = x - x_{\text{clim}}$. This way, also periodic changes due to seasonality are removed. (6) Afterwards, to reduce the noise caused by natural variability, which might lead to overfitted models, the data is smoothed out via a 7-day centred rolling mean. (7) Then, we standarize the predictors: $x_{\text{std anom}} = \frac{x_{\text{anom}}}{x_{\text{std}}}$, where $x_{\text{std anom}}$ are the standarized anomalies and x_{std} is the standard deviation of the distribution of each predictor. (8) Furthermore, for each of the six prediction lead times (1–6 weeks), the predictors are given to the ML models at four different time lags before initialization time. For example, for a forecast at two weeks lead time (meaning that we are using a model initialized at a lag of two weeks to forecast *temperature* at lag zero), the *precipitation* (p) is provided at lags of two to five weeks (i.e., p_{lag2}, p_{lag3}, p_{lag4}, and p_{lag5}). (9) Finally, since we want to investigate the predictability of summer temperature, only the extended summer months (MJJAS) are selected.

c. Data balance

Forecasting of the two weekly summer heatwave indices defined in Section 3a ($+1\sigma$ and $+1.5\sigma$) results in an imbalanced classification problem. Using these two indices, we obtain imbalanced training sets (e.g., for the $+1.5\sigma$ index, only 7.41 % of the samples belong to the positive class). A classifier trained on these imbalanced data will learn to always forecast the negative class, leading to a trivial model. Balancing the data before the training and optimizing the probability threshold (see

Sec 3f) are two potential solutions to this problem. For this study, we find that the combination of both methods yields the best results. Therefore, an additional data-balancing step must be added by the end of the preprocessing pipeline (see Sec 3b2). Two different approaches have been explored and are compared in this study: (1) We **undersample** the dataset by selecting a random subset of examples from the negative class, to obtain a 50/50 ratio between positive and negative classes (Lemaitre et al. 2017). Yet, the size of the training set is considerably reduced by doing so (e.g., from 4'437 training samples to 658 for the *+1.5*σ index). (2) Alternatively, we **oversample** the dataset by repeating randomly selected examples from the positive class until a 50/50 ratio between positive and negative classes is achieved (Lemaitre et al. 2017). This approach increases the size of the training set (e.g., from 4'437 points to 8'216 for the *+1.5*σ index), although the number of independent samples remains the same. The same information for the *+1*σ index is provided in Table 3.

Weekly heatwave index	***+1*σ**	***+1.5*σ**
Percentage of samples in the positive class	20.0%	7.41%
Number of training samples (undersampling)	1'772	658
Number of training samples (oversampling)	7'102	8'216

TABLE 3: **Data balance** Size of the full training set (initially with 4'437 samples) after under-/ and oversampling.

d. Machine Learning models

For our study, we choose models at the two extremes of the bias-variance tradeoff (Mehta et al. 2019). (1) The more simple linear models are prone to have high bias, meaning that the model will match the training set less closely. These models have a higher potential for under-fitting. Linear models, however, have low variance, meaning that the predictions of the model do not fluctuate much with a change of dataset. Overall, these models are focused on the larger trends rather than on the complicated patterns of the training set. (2) Instead, the more complex RFs are likely to overfit the data, but also to capture most of the relevant patterns. They tend to have high variance, but low bias. Here, two models out of each of these two families are used for the regression and classification forecasts. The multilinear regression (MLR) and the ridge classifier (RC) belong to the *linear model*, and the random forest regressor (RFR) and the random forest classifier (RFC) belong to the *ensemble* modules from *Sklearn*, respectively (Pedregosa et al. 2011).

1) Linear Models

Linear regression models forecast the target y as a linear combination of n predictors x_i:

$$\hat{y}(\boldsymbol{\omega}, \boldsymbol{x}) = \omega_0 + \omega_1 x_1 + ... + \omega_n x_n \tag{1}$$

where ω_0 is the intercept and ω_i $(0 < i \leq n)$ are the regression coefficients. The coefficients are chosen to minimize the residual sum of squares between the forecast ($\hat{y}$) and the observed target (y): $min_{\boldsymbol{\omega}}||\hat{y} - y||$. Linear classification models first convert binary targets to {-1, 1} and then treat the problem as a regression task. The forecasted class corresponds to the sign of the regressor's forecast. For classification, we use Ridge regularization to control excessively fluctuating functions by adding an additional penalty term in the error function, such that the coefficients do not take extreme values (Mishra 2018). Ridge shrinks the predictor coefficients based on the L2-norm ($||\boldsymbol{x}||_2 = \sqrt{\sum_i x_i^2}$). The loss function for minimization then becomes $||\hat{y} - y|| + \alpha||\boldsymbol{\omega}||_2^2$, where the complexity parameter α is a hyper-parameter which controls the amount of shrinkage and is set to 1.0.

2) Random forests

A decision tree makes a recursive partition of the input space into rectangles, by selecting the predictor and the respective cutting point that discriminate best at each node. The resulting leaves (i.e., final nodes) correspond to a specific forecast value (regression) or to a probability of belonging to the positive class (binary classification). However, decision trees have two key disadvantages: (1) Trees usually have high variance due to their greedy split process, which implies that a small change in training data can result in significantly different splits. (2) Since the tree estimate is not smooth, decision trees may not be appropriate when the underlying function is smooth (Khan et al. 2019). A more accurate and robust model can be constructed by creating a random ensemble of uncorrelated decision trees whose averaged prediction is more accurate than that of any individual tree. Random forests use two sources of randomness while training: bagging and feature randomness. (1) Bagging (or bootstrap aggregation) consists in selecting a random subset of the training set with replacement – meaning that individual data points can be chosen more than once – to train each individual tree. (2) When splitting a node in a classical decision tree, all features are considered and the one that provides the greatest separation between observations is selected. In contrast, each individual tree in a RF can pick only from a random subset of features (Yiu 2019). Finally, the mean or majority-vote forecast of all the regression or classification trees in the forest is selected as the final result, respectively. RFs are chosen over other tree-based algorithms, since they are more interpretable (Rudin 2019) than XgBoost and less prone to overfit than single decision trees.

e. Metrics for the evaluation of forecasting performance

For regression, two different metrics are considered: root mean-square error (RMSE) and Pearson correlation. The RMSE evaluates how far away the forecasted and the ground truth curves are from each other and is defined as:

$$\mathrm{RMSE} = \sqrt{\mathrm{MSE}} = \sqrt{\frac{1}{T}\sum_{t=1}^{T}(\hat{y}_t - y_t)^2} \tag{2}$$

for y_t the regression dependent variable at time t, $\hat{y}_t$ the predicted value for time t, and T the number of time steps (sample size). The Pearson correlation measures to what extent the curve follows the changes and is given by:

$$\mathrm{Corr} = \frac{\sum_{t=1}^{T}(\hat{y}_t - \bar{\hat{\boldsymbol{y}}})(y_t - \bar{\boldsymbol{y}})}{\sqrt{\sum_{t=1}^{T}(\hat{y}_t - \bar{\hat{\boldsymbol{y}}})^2}\sqrt{\sum_{t=1}^{T}(y_t - \bar{\boldsymbol{y}})^2}} \tag{3}$$

for $\bar{\boldsymbol{x}} = \frac{1}{T}\sum_{t=1}^{T} x_t$ the sample mean (i.e., mean over all time steps).

For classification, the Receiver Operating Characteristic (ROC) Area Under Curve (AUC) is used to evaluate the probabilistic forecast. The ROC is the true positive rate (TPR) as a function of the false positive rate (FPR) (Bradley 1997). The TPR (or Recall) is defined as the proportion of positive data points that are correctly considered as positive, with respect to all positive data points. The TPR is given by TP/ (FN+TP) for true positives (TPs) and false negatives (FNs). The FPR (or False Alarm) is defined as the proportion of negative data points that are mistakenly considered as positive, with respect to all negative data points. The FPR is calculated as FP / (FP+TN) for false positives (FPs) and true negatives (TNs). Moreover, the performance of the binary classification is assessed via the confusion matrix (see Tab 4) and the geometric mean of the TPR and the FPR (G-Mean), which is defined as G-Mean = $\sqrt{TPR(1-FPR)}$ (Brownlee 2020).

We define a *useful* forecast as having a ROC AUC above 0.5 for the probabilistic forecast and a TPR higher than the FPR for the binary classification. For a sensible model, the principal diagonal element values must be high and the off-diagonal element values must be low in the confusion matrix (Bradley 1997).

		Actual value	
		Positive (1)	Negative (0)
Forecasted value	Positive (1)	TP	FP
	Negative (0)	FN	TN

TABLE 4: **Confusion matrix** The positive class corresponds to a heatwave and the negative class to no heatwave.

f. Cross-Validation and hyper-parameter optimization

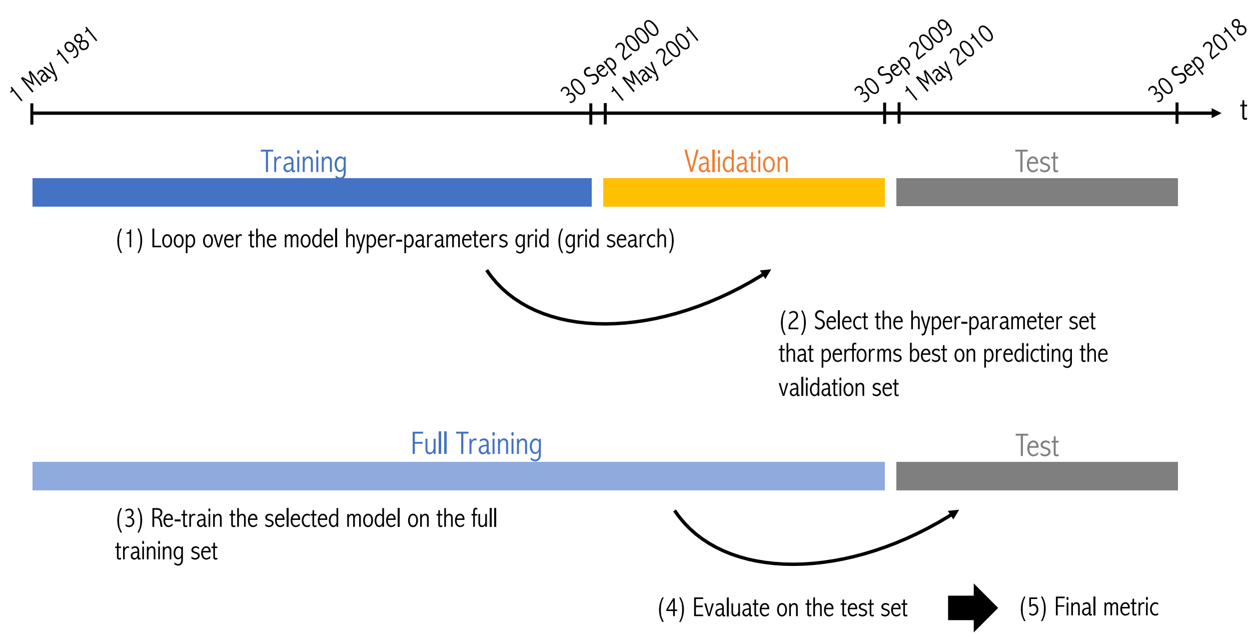

FIG. 3: **Schematic of the training-validation-test splits**

We split the available data into a training period (1 May 1981 – 30 September 2000), a validation period (1 May 2001 – 30 September 2009), and a testing period (1 May 2010 – 30 September 2018) (see Fig 3). The validation period is used to optimize the model's hyper-parameters. After the hyper-parameter optimization, the model is re-trained on the full training period (1 May 1981 – 30 September 2009), which is the combination of the validation and the training period. A nested cross-validation (CV) scheme is also implemented (see Fig A1 in the Appendix).

For the RFs, we use an exhaustive grid-search hyper-parameter optimization including all possible combinations (750) of the following parameters: number of trees in the forest $\in \{50, 100, 200, 400, 600\}$, maximum tree depth $\in$ 5–14, and a range of 15 values centered around the training set's length divided by 100 for the minimum number of samples per leaf. The minimum number of samples for splitting a node is set to the minimum number of samples per leaf multiplied by a factor of two. The reference metrics for optimization are the RMSE for regression and the ROC AUC for classification. Moreover, the classification models output a probability for each validation sample to belong to the positive class. Then, the probability threshold between zero and one that maximises G-Mean is selected to binarize the output (Brownlee 2021; Swets et al. 2000). No hyper-parameter tuning is needed for the two linear models (MLR and RC).

g. Lead time

We forecast at 1–6 weeks lead time. The models are trained separately for each lead time and do not learn from each other. For instance, the two weeks lead time forecast does not receive the one week lead time forecast as an additional input. Moreover, since our data is averaged via a seven-day rolling mean (see Sec 3b2), weeks are labeled by their central day. A one-week-lead-time prediction leaves no gap between the days used to calculate the one-week lag predictors and the days used to determine the target. For instance, the one-week-lead-time forecast run on June 4th (average over June 1st–June 7th) forecasts June 11th (average over June 8th–June 14th). Similarly, two weeks lead time leave a gap of seven unused days.

h. Reference forecasts

We compare our models' performance to the (1) climatology, (2) persistence, and (3) ECMWF re-forecasts (hindcasts). (1) For the regression problem, *temperature* anomalies with respect to climatology are forecasted. Thus, the climatology forecast is zero for all times per definition. For the classification problem, we compute the climatology forecast as the mode class for each day of the year. Since, in our dataset, the negative class strongly predominates over the positive class, the climatology forecast is found to be the negative class (no heatwave) for all days of the year. (2) Persistence forecasts predict that the future weather condition will be the same as the present condition. In practice, the persistence forecast is defined as keeping the value from initialization time until verification time. For instance, for the regression forecast at two weeks lead time, the persistence is the *temperature* anomaly two weeks before verification time. (3) The ECMWF sub-seasonal prediction system is initialized twice a week and provides 20-year hindcasts with 11 ensemble members integrated over 46 days. The hindcasts used here cover the period 2000–2019 and use the model version of the Integrated Forecasting System (IFS) cycle 47r1 (Haiden et al. 2019). We use the *temperature* anomalies of the ensemble mean as a reference forecast. The *temperature* anomalies are calculated by removing the lead time dependent climatology at each initialization, calculated by the 20-year mean of the 11-member ensemble started on the same day and month for each year of the reference period (2000–2019). For instance, if a hindcast was initialized on the 31st of May, the lead time dependent climatology corresponding to that hindcast is calculated by the mean of the 11-member ensemble initialized on the 31st of May and averaged over the 20-year reference period (2000–2019) separately for each of the 46 days. For each initialization, after the calculation of the *temperature* anomalies, a 7-day rolling mean was applied. In this way, we end up with 40 days per initialization, with each day being the centre of the 7-day rolling mean. For instance, the first day predicted by the initialization on the 31st of May will be June 4th (average over June 1st–June 7th).

i. Uncertainty estimation

We use the standard deviation of a model ensemble to quantify the uncertainty of the forecasts by the ECMWF and the ML models. For ECMWF, the considered ensemble consists of 11 models. For the RFs, the forecasts by the individual trees in the forest are used. Depending on the hyper-parameter optimization, the number of estimators forming the ensemble can vary between ten and 600. Finally, for the linear models, an ensemble of 600 members is created by randomly removing five full (but not necessarily sequential) years from the full training set.

4. Results and discussion

a. Forecasts

1) Regression forecasts

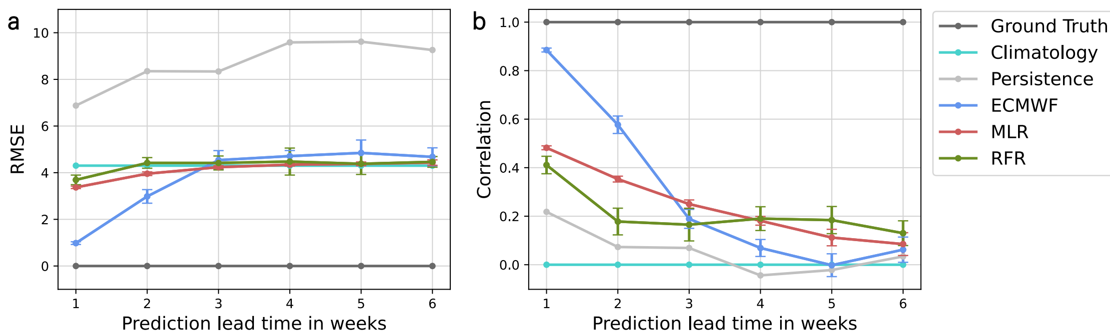

Fig. 4: **Performance of the regression models for six different lead times** (a) RMSE and (b) correlation for the regression forecasts. An accurate forecast is characterized by a low RMSE and a high correlation. The error bars show the uncertainty of each forecast estimated via the standard deviation of the ensemble mean.

In Figure 4, the regression forecasts from two different ML models (MLR and RFR) at six different lead times (1–6 weeks) are compared among each other and to the climatology, persistence, and ECMWF forecasts. The analogous results for nested CV are shown in Figure A2 in the Appendix. As can be observed in Figure 4, all metrics are best for a lead time of one week. The uncertainty in the forecasts by all models, which is represented by the error bars, increases with lead time. For the linear ML model, the performance decays linearly with increasing lead time, with a correlation that ranges from 0.48 for one week lead time to 0.09 for six weeks lead time. For the RF, the correlation decreases overall from one to six weeks lead time (from 0.41 to 0.13), but remains noticeably constant for lead times longer than one week. The evolution of the RMSE is similar, but with the difference that it saturates when reaching the RMSE value that corresponds to the climatology forecast. The RMSE for the best model at each lead time ranges between 3.37 for one week lead time and 4.43 at six weeks lead time.

The linear ML model outperforms the RF at short lead times (up to three weeks), but the RF model provides a better forecast at long lead times (5–6 weeks). Both ML models outperform the persistence forecast at all lead times. However, the climatology forecast has a relatively low RMSE, since zero variability is a good guess at long lead times, when forecasting becomes difficult. For lead times longer than two weeks, the RMSEs of the ML models saturate at the climatology's RMSE and ECMWF has a worse RMSE than the climatology forecast. Still, the climatology forecast does not correlate with the ground truth and the ML and ECMWF models outperform climatology at all lead times in terms of correlation, since the models always correlate positively with the ground truth. While ECMWF provides highly skilled forecasts in terms of correlation and RMSE for one and two weeks lead time, the skill decreases fast with increasing lead time; for lead times of three weeks and longer, the ML models forecast the temperature anomalies more accurately than ECMWF.

The ML models generally pick up the sign of the anomalies but their variability is lower than the one from ECMWF and extreme values are not well-captured (see Fig C1 in the Appendix). For longer lead times, all models lose variability, tending to the climatology forecast. In the case of the ML models, this tendency towards climatology can be a consequence of the loss function. The loss functions for the MLR and the RFR models are the residual sum of squares and the mean-square error, respectively. For the hyper-parameter optimization, the RMSE is used. All three metrics measure the distance between the forecast and the target curves. Since forecasting anomalies accurately becomes more difficult with increasing lead time, a model that is trained to minimise the error will tend to forecast the mean of the distribution of possible outcomes, becoming smoother and losing variability compared to the observations (Rasp and Thuerey 2021). ML models trained to optimize alternative loss functions (e.g., the correlation) would be worth exploring.

2) Classification forecasts

The classification models output a probability for each sample in the test set to belong to the positive class (i.e., for a week to be classified as a heatwave week). This probabilities are then binarized via a probability threshold, meaning that a zero (no heatwave) or a one (heatwave) is assigned to each sample in the test set (see Sec 3f). In Figure 5, the probabilistic classification forecasts from two different ML models (RC and RFC) at six different lead times (1–6 weeks) are compared among each other and to the climatology, persistence, and ECMWF forecasts. In Figure 6, the performance of the binary classification forecasts is shown. The analogous results for nested CV are shown in Figures A3 and A4 in the Appendix. Two different indices are used: $+1\sigma$ for warm and $+1.5\sigma$ for extremely warm temperatures (see Sec 3a for the index definitions).

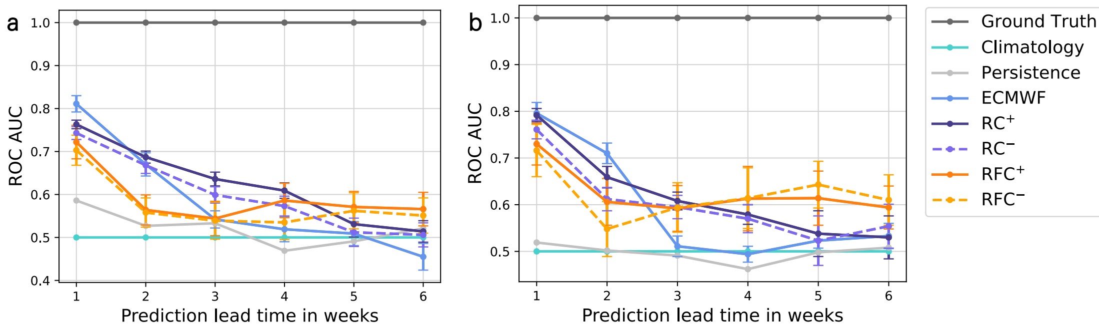

FIG. 5: **Performance of the probabilistic classification models for six different lead times** ROC AUC for the (a) *+1σ* and (b) *+1.5 σ* weekly heatwave index. An accurate probabilistic classification forecast is characterized by a high ROC AUC. A no-skill probabilistic classification forecast is represented by a ROC AUC of 0.5, indicated by the climatology. The error bars show the uncertainty of each forecast estimated via the standard deviation of the ensemble mean. Notation: x^{+}: oversampled and x^{-}: undersampled.

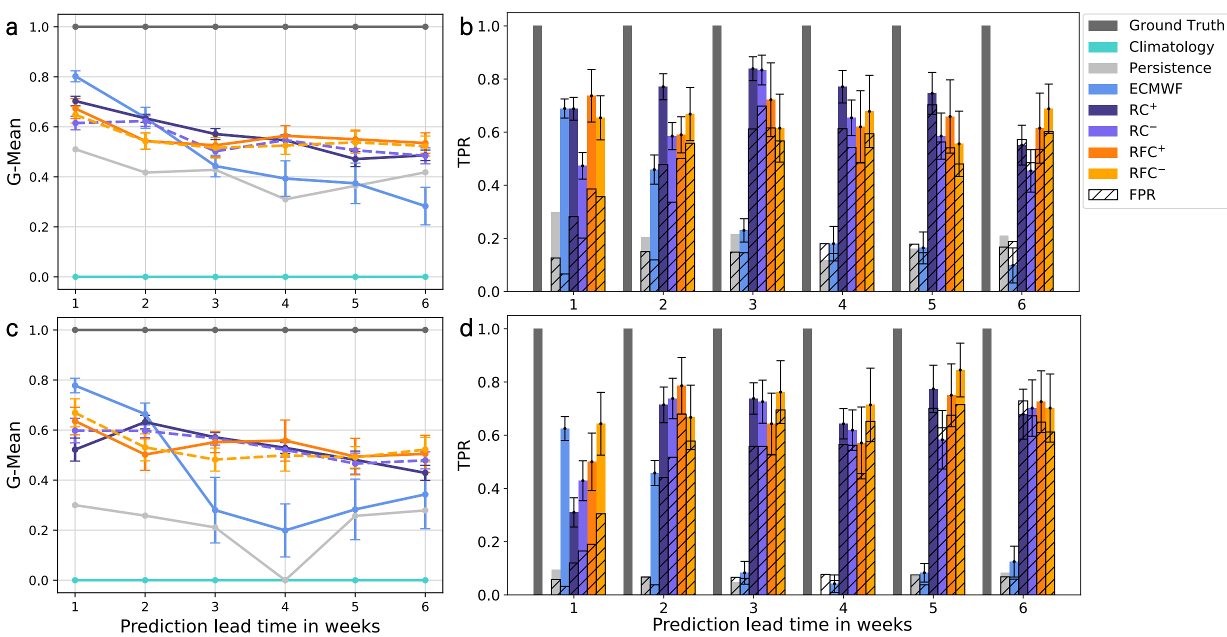

FIG. 6: **Performance of the binary classification models for six different lead times** (a) G-Mean and (b) TPR for the *+1σ* weekly heatwave index. (c) and (d) are the corresponding forecasts for the *+1.5 σ* weekly heatwave index. An accurate binary classification forecast is characterized by a high G-Mean. A no-skill binary classification forecast is represented by a G-Mean of zero. The stippled bars in (b) and (d) represent the FPR or False Alarm Rate. The error bars show the uncertainty of each forecast estimated via the standard deviation of the ensemble mean. Since the climatology forecast predicts only zeros (no heatwave), both its TPR and FPR are equal to zero for all lead times. Notation: x^{+}: oversampled and x^{-}: undersampled.

The influence of the technique used to balance out the data is also assessed: we compare the performance of the models when trained on an undersampled (x^{-}) and on an oversampled (x^{+})

dataset. Models trained on an unbalanced dataset (with optimized probability threshold) had a slightly lower overall performance (not shown).

In general, the linear models have a higher skill than the RFCs for short lead times (up to three weeks). However, two RFCs have a skill that remains more constant than the linear models' skill across lead times and they therefore outperform the linear models for lead times longer than four weeks. Also, the uncertainty in the forecasts by all models increases with lead time. These patterns are analogous to the ones observed for the regression forecast (see Fig 4b). The performance of the best probabilistic forecast decays considerably as the lead time increases (see Fig 5a&b). The ROC AUC for the best model at each lead time is shown in Table 5. Instead, the performance of the best binary classification forecast is more stable, although it also decreases with lead time (see Fig 6a&c). Nevertheless, at least one ML model provides a *useful* forecast at each of the considered lead times (1–6 weeks). Meant by *useful* is a ROC AUC above 0.5 for the probabilistic forecast (see Fig 5a&b) and a TPR higher than the FPR for the binary classification (see Fig 6b&d). It is remarkable that non-null skill is present at these long lead times.

As for regression, the classification ML models outperform persistence and climatology at all lead times. The persistence forecast has a higher skill when predicting high temperature anomalies ($+1\sigma$) than when predicting extremely high temperature anomalies ($+1.5\sigma$). Our models yield more accurate forecasts than ECMWF for lead times longer than two weeks. At these longer lead times, ECMWF predicts fewer weekly heatwave events than the ML models, having a lower TPR and FPR (see Fig 6b&d). Furthermore, the difference in skill between the ML and ECMWF forecasts at these longer lead times is, in general, more pronounced for the $+1.5\sigma$ index than for $+1\sigma$. The performance of ECMWF in predicting extremely high temperature anomalies ($+1.5\sigma$) drops drastically between two and three weeks lead time. In contrast, ECMWF's classification skill when forecasting high temperature anomalies ($+1\sigma$) decays close to linearly with lead time. Finally, while the oversampled models perform slightly better than the undersampled models for forecasting the $+1\sigma$ weekly heatwave index, there is no clear evidence for one data balancing technique being superior across different indices.

Weekly heatwave index	1 week	2 weeks	3 weeks	4 weeks	5 weeks	6 weeks
+1σ	0.76 (RC$^+$)	0.69 (RC$^+$)	0.64 (RC$^+$)	0.61 (RC$^+$)	0.57 (RFC$^+$)	0.57 (RFC$^+$)
+1.5σ	0.79 (RC$^+$)	0.66 (RC$^+$)	0.61 (RC$^+$)	0.61 (RFC$^-$)	0.64 (RFC$^-$)	0.61 (RFC$^-$)

TABLE 5: **ROC AUC scores for the best models** The best model among RC$^+$, RC$^-$, RFC$^+$, and RFC$^-$ is chosen for the forecast of each weekly heatwave index at each lead time.

b. Predictor importance

In this section, the relevance of each of the seven predictors for forecasting summer temperature anomalies is discussed. First, a linear correlation analysis is performed. Second, we investigate which lagged predictors were predominantly used by each ML model.

1) LINEAR CORRELATION ANALYSIS

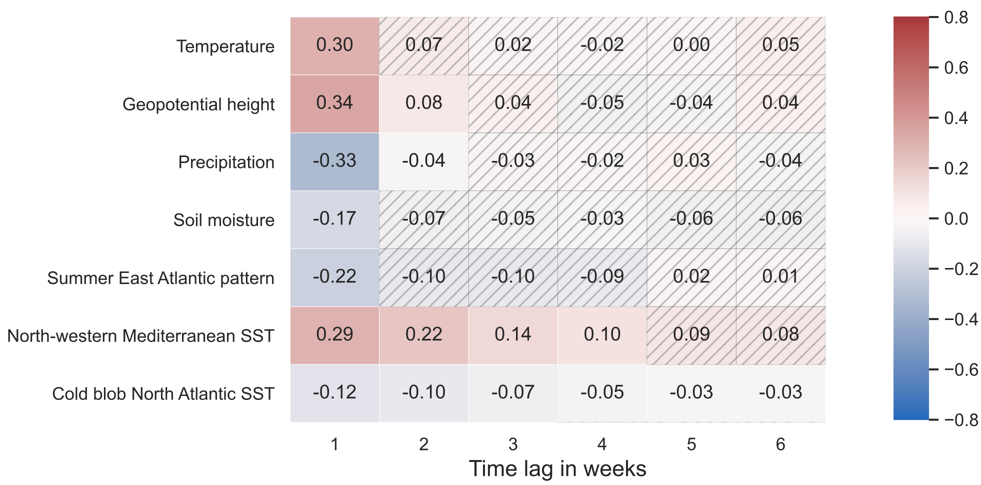

FIG. 7: **Lagged linear correlations between the predictors and the *temperature*** in the extended summer season (MJJAS) at weekly time resolution. When trained with MJJAS data only, our ML models predict summer temperature anomalies and heatwaves with higher accuracy than if the full year is used. Hatched cells correspond to non-significant linear correlations at 5% significance level.

In Figure 7, the linear correlations between the *temperature* and the predictors in the extended summer season (MJJAS) are shown for six different time lags (1–6 weeks). At short time lags, the *temperature* shows a strong autocorrelation. The *geopotential* has an even stronger positive correlation to the *temperature*, indicating that during anticyclonic conditions higher temperatures than normal are expected. In contrast, *precipitation*, *soil moisture*, and the *SEA* correlate negatively with *temperature* at short time lags. *Precipitation* is associated with cyclones, cloudy conditions, and lower surface air temperatures (see Sec 2). Moreover, dryness (low *soil moisture*) and high *temperature* reinforce each other (see Sec 2). The correlations with the atmospheric predictors (*temperature*, *geopotential*, *precipitation*, and *SEA*) decay fast. In addition, the linear correlation with *soil moisture* becomes non-significant for lead times of two weeks and longer. In contrast, the SST predictors show a more constant linear correlation over time and dominate on time scales longer than a week, since they are more persistent. While the *NWMED SST* correlates positively with the *temperature* over CE, the *CNAA SST* correlates negatively with both.

2) Relevance of lagged predictors for the Machine Learning models

Each of the seven predictors is provided to the ML models at four time lags, building a set of 28 lagged predictors for each lead time (see Sec 3b2). The relevance of a lagged predictor for each ML model is given by the absolute value of its correlation coefficient for the linear models and its feature importance for the RF models. These values are shown in Tables B1 and B2 for the linear models (MLR and RC^+, respectively) and in Tables B3 and B4 for the RFs (RFR and RFC^+, respectively) (see Appendix).

In general, predictors at short lags are more useful to the models. Also, the longer the forecast's lead time, the higher the contribution from SST becomes. When forecasting the $+1\sigma$ and the $+1.5\sigma$ heatwave indices, the set of relevant lagged predictors is similar. Nevertheless, we can find differences between the two families of models. For instance, the linear models rely more on SSTs than the RFs.

(i) Linear models For the linear models, SSTs dominate at all lead times. In particular, the *CNAA SST* is the most relevant predictor for the MLR model at all lead times. Nonetheless, the *temperature*, the *precipitation*, and the *soil moisture* at short lags are useful predictors for the MLR model at short lead times (1–2 weeks) as well. In contrast, these lagged predictors are not of use for the RC^+ model, which relies almost exclusively on SSTs.

(ii) RF models For the RF models, *temperature*, *geopotential*, *precipitation*, the *SEA* index, and *NWMED SST* at short lags are the most important predictors at short lead times (one week). SSTs are found to dominate for longer lead times (2–6 weeks), without a substantial difference between *CNAA SST* and *NWMED SST*. In addition, *soil moisture* and the *SEA* index are useful at lead times

of 3–6 and 1–5 weeks, respectively. At lead times longer than one week, these two predictors have no significant linear correlation with the *temperature* (see Fig 7) and are used by the RF models but not by the linear models. A plausible explanation for this phenomenon is the presence of highly non-linear links between *temperature* and *soil moisture*, and *temperature* and the *SEA* index. The physical mechanism behind the non-linear link between *temperature* and *soil moisture* can be the positive feedback loop described in Section 2. In addition, a non-linear summer atmospheric response to the SEA pattern in Europe was found by Ossó et al. (2020). The SEA pattern might also influence temperature indirectly through surface-atmosphere feedbacks (including soil moisture). These two non-linear links between *temperature* and *soil moisture*, and *temperature* and the *SEA* index would explain the enhanced skill of the RF models compared to the linear models at lead times higher than four weeks (see Sec 4a).

5. Limitations and downstream tasks

In this section, further research ideas to improve the forecast's accuracy are suggested: (1) promising alternative models, and (2) approaches to overcome the limitations due to a small sample size.

(1) The models used in our study belong to the field of classical ML. The complex nature of climate data (e.g., non-linear dependencies between predictors, autocorrelation, and unobserved predictors) poses important challenges to traditional ML models. As discussed in Section 1, DL is also being used for extreme weather forecasting. DL can capture more complex relationships between predictors and target, and might therefore be better suited to describe the mechanisms behind heatwaves, which most likely include non-linear processes. In addition, classical ML approaches benefit from domain specific hand-crafted features to account for dependencies in time or space, but rarely exploit spatio-temporal dependencies exhaustively. In contrast, DL can automatically extract abstract spatio-temporal features (Reichstein et al. 2019). Yet, DL models require larger datasets than the ones used for this study and were therefore not used.

(2) One of the main limitations of this study is the size of the dataset. The initial dataset is considerably larger, but precious information gets lost when taking the average over latitude-longitude boxes. It might be interesting to explore the effect of using several smaller sub-boxes instead of one large box. Additional columns could be added to the dataset, such as a box label

or its latitude-longitude coordinates. Also, the currently used boxes are rectangular and their coordinates are chosen based on our physical understanding and the correlation to the target. This could be refined by letting an algorithm select sub-regions of different shapes for each predictor based on the correlation of each grid cell to the target (Vijverberg et al. 2020) or even including the spatial information of the predictors (van Straaten et al. 2022). While lower-dimensional models like MLR and RC might not be able to distinguish between distinct mechanisms acting in different regions, RFs are expected to benefit from additional data.

6. Conclusions

To conclude, we return to the two research questions about the relevant predictors for summer temperature and the potential improvements of heatwave prediction through ML methods, as stated in the Introduction (see Sec 1):

(i) At short lead times (1 week), the following variables are found to be the best predictors of summer temperature anomalies and heatwaves in CE: local 2-m air *temperature*, 500-hPa *geopotential*, *precipitation*, and *NWMED SST*. At longer lead times (2–6 weeks), *NWMED* and *CNAA SST* are the most relevant predictors. Moreover, the *SEA* index and *soil moisture* have a linear link with *temperature* at one week lead time and a possible non-linear link at longer lead times (see Sec 4b).

(ii) The performance of the linear and RF models used for forecasting summer temperature anomalies and heatwaves in CE decays with lead time but outperforms persistence and climatology at all lead times. ECMWF yields accurate forecasts for 1–2 weeks lead time but our ML models beat ECMWF at lead times longer than two weeks. While the linear models perform better for shorter lead times (1–3 weeks), the RFs take over at lead times longer than four weeks. The regression forecast of summer temperature is better than a random prediction in forecasting the sign of the anomalies at all considered lead times (1–6 weeks). However, extreme values are poorly captured. For the classification problem, at lead times longer than two weeks, the difference in skill between the ML and ECMWF forecasts is more pronounced for extremely warm temperatures ($+1.5\sigma$) than for warm temperatures ($+1\sigma$). At least one out of the ML models yields a *useful* forecast (meaning ROC AUC > 0.5 and TPR > FPR) for each of the considered lead times (1–6 weeks) (see Sec 4a). It is remarkable that non-null skill is present at these long lead times.

In summary, we show that ML models can help extend the forecasting lead time of summer temperature anomalies and heatwaves to sub-seasonal scales. ML methods are a promising direction for further research in sub-seasonal forecasting. Nevertheless, making better forecasts is not enough. Forecasts acquire value through their ability to influence the decisions made by their users (Murphy 1993). As discussed in the Introduction (see Sec 1), EWS involve not only forecasting the heatwave event, but also triggering effective and timely response plans that target vulnerable populations and regions. This second step must also be successfully implemented to reduce the impact of such damaging events (Merz et al. 2020; White et al. 2021).

Acknowledgments. This project has received funding from the European Research Council (ERC) under the European Union's Horizon 2020 research and innovation programme (project "HEAT-forecast", Grant agreement No. 847456). Support from the Swiss National Science Foundation through projects PP00P2_170523 and PP00P2_198896 to Maria Pyrina and Daniela Domeisen is gratefully acknowledged. Judah Cohen is supported by the US National Science Foundation grants AGS-1657748 and PLR-1901352. We thank Ole Wulff for downloading a part of the data used for this study. Also, we appreciate the recommendations from Michael Murphy and Achim Baldus Benet. Finally, we acknowledge Liam Grunwald for improving the English in the manuscript. The authors declare no conflicts of interests.

Data availability statement. We acknowledge the E-OBS dataset from the EU-FP6 project UERRA[1] and the Copernicus Climate Change Service, and the data providers in the ECA&D project (Cornes et al. 2018).[2] The ERA-Interim (Dee et al. 2011), ERA5-Land (Muñoz-Sabater et al. 2021), and ERA20C (Poli et al. 2016) data are provided by ECMWF.[3] The HadISST data are provided by the Met Office Hadley Centre (Rayner et al. 2003). The ECMWF S2S data are publicly accessible.[4]

[1]https://www.uerra.eu
[2]https://www.ecad.eu
[3]www.ecmwf.int
[4]https://apps.ecmwf.int/datasets/data/s2s

APPENDIX A

Nested Cross-Validation

To assess the robustness of our ML models, a CV scheme is implemented. In CV, the model is trained on different data subsets, which reduces overfitting and results in a better generalisation. Moreover, CV removes the dependency on an arbitrarily-selected test set (i.e., from decadal variability here), making the metrics more robust (Vabalas et al. 2019). Here, a nested CV scheme with five outer and two inner splits is used (see Fig A1). The main benefit of nested CV compared to other CV schemes is that the model is trained and tested on the full dataset while maintaining the independence of the test set. This method is, therefore, well-suited for a limited sample size.

Nested CV is generally not used for time series data, since consecutive time steps are strongly correlated. However, since the correlation between the considered predictors decays after a maximum of a few months and only summer data points are selected for this study, summers belonging to different years can be considered independent from each other. To avoid a strong correlation between the sets at the splitting points, the data is split during the winter months.

FIG. A1: **Nested cross-validation scheme** Figure adopted from Vabalas et al. (2019).

The metrics obtained with nested CV (see Figs A2, A3, and A4) are similar, although smoother, compared to the results without CV (see Figs 4, 5, and 6 in Sec 4). The linear models also show a higher skill than the RF models for lead times up to three weeks and the RFs outperform the linear models at 5–6 weeks lead time. While the skill of the ML models at short lead times (up

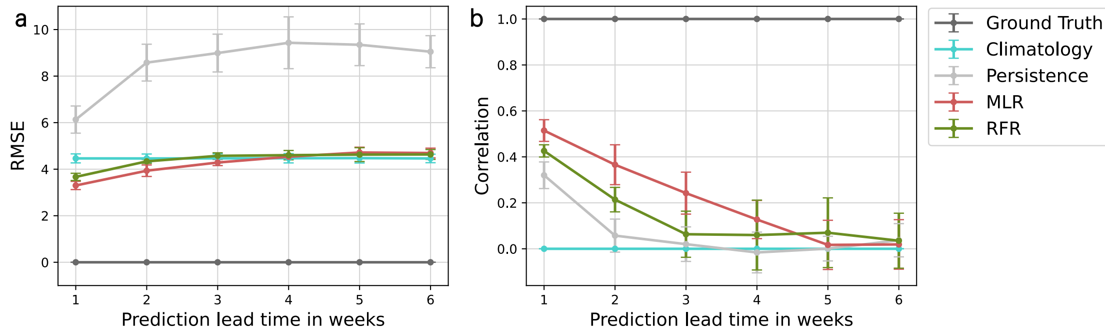

Fig. A2: **Performance of the regression models for six different lead times with nested CV** (a) RMSE and (b) correlation for the regression forecasts. An accurate forecast is characterized by a low RMSE and a high correlation. The error bars show the uncertainty of each forecast estimated via the standard deviation of the ensemble mean.

to three weeks) is similar with and without CV, the models in nested CV perform slightly worse for longer lead times. Moreover, the uncertainty of the ML models is higher with nested CV than without. Therefore, while at least two ML models outperform persistence and climatology in average for all lead times, the error bars overlap with the reference forecasts for lead times of three weeks and longer. A comparison to the ECMWF forecast can not be included for nested CV, because the dynamical model is not available during the full test period used for these CV scheme (1981–2018). Furthermore, the binary classification forecast is found to be considerably better than the probabilistic classification forecast compared to the reference forecasts. Finally, the difference between the two data balance methods (under-/ and oversampling) is considerably dampened by the nested CV and the two approaches can be considered almost equivalent.

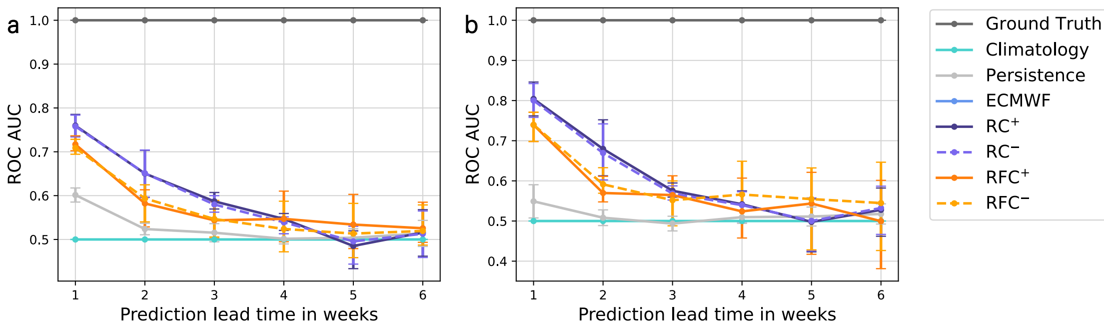

FIG. A3: **Performance of the probabilistic classification models for six different lead times with nested CV** ROC AUC for the (a) $+1\sigma$ and (b) $+1.5\ \sigma$ weekly heatwave index. An accurate probabilistic classification forecast is characterized by a high ROC AUC. A no-skill probabilistic classification forecast is represented by a ROC AUC of 0.5, indicated by the climatology. The error bars show the uncertainty of each forecast estimated via the standard deviation of the ensemble mean. Notation: x^{+}: oversampled and x^{-}: undersampled.

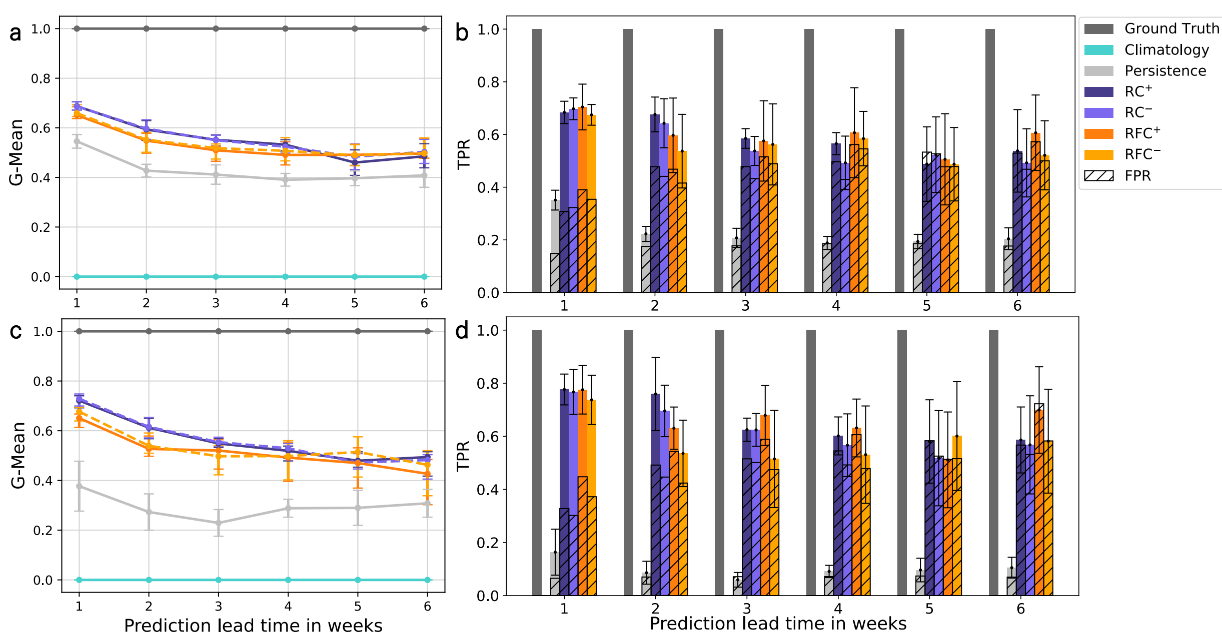

FIG. A4: **Performance of the binary classification models for six different lead times with nested CV** (a) G-Mean and (b) TPR for the $+1\sigma$ weekly heatwave index. (c) and (d) are the corresponding forecasts for the $+1.5\ \sigma$ weekly heatwave index. An accurate binary classification forecast is characterized by a high G-Mean. A no-skill binary classification forecast is represented by a G-Mean of zero. The stippled bars in (b) and (d) represent the FPR or False Alarm Rate. The error bars show the uncertainty of each forecast estimated via the standard deviation of the ensemble mean. Since the climatology forecast predicts only zeros (no heatwave), both its TPR and FPR are equal to zero for all lead times. Notation: x^{+}: oversampled and x^{-}: undersampled.

APPENDIX B

Correlation coefficients and feature importances

Lead time		1 week	2 weeks	3 weeks	4 weeks	5 weeks	6 weeks
Predictor	**Lag (weeks)**						
Temperature	1	0.47	-	-	-	-	-
	2	-0.4	-0.3	-	-	-	-
	3	-0.23	**-0.51**	-0.42	-	-	-
	4	0.05	0.02	-0.07	-0.12	-	-
	5	-	0.26	0.35	0.31	0.25	-
	6	-	-	0.2	0.33	0.29	0.31
	7	-	-	-	-0.3	-0.22	-0.14
	8	-	-	-	-	-0.15	-0.08
	9	-	-	-	-	-	-0.07
Geopotential	1	0.07	-	-	-	-	-
	2	0.21	0.21	-	-	-	-
	3	0.14	0.33	0.26	-	-	-
	4	-0.21	-0.17	-0.14	-0.12	-	-
	5	-	-0.3	-0.39	-0.36	-0.39	-
	6	-	-	-0.18	-0.35	-0.31	-0.32
	7	-	-	-	0.3	0.15	0.08
	8	-	-	-	-	0.25	0.18
	9	-	-	-	-	-	0.15
Precipitation	1	**-0.66**	-	-	-	-	-
	2	0.07	0.22	-	-	-	-
	3	0.21	0.27	0.3	-	-	-
	4	-0.03	0.02	0.04	-0.02	-	-
	5	-	-0.05	-0.05	0.03	-0.04	-
	6	-	-	-0.1	-0.01	0.04	-0.05
	7	-	-	-	0.08	0.17	0.13
	8	-	-	-	-	0.2	0.28
	9	-	-	-	-	-	0.33
Soil moisture	1	**0.94**	-	-	-	-	-
	2	**-0.65**	-0.08	-	-	-	-
	3	-0.24	-0.28	-0.39	-	-	-
	4	0.03	0.08	-0.04	-0.33	-	-
	5	-	0.03	0.14	-0.01	-0.27	-
	6	-	-	0.08	0	-0.05	-0.17
	7	-	-	-	0.18	-0.06	-0.06
	8	-	-	-	-	0.17	-0.11
	9	-	-	-	-	-	0.03
SEA	1	-0.05	-	-	-	-	-
	2	-0.01	-0.04	-	-	-	-
	3	-0.14	-0.12	-0.12	-	-	-
	4	-0.11	-0.14	-0.14	-0.16	-	-
	5	-	0.17	0.19	0.24	0.19	-
	6	-	-	0.03	0.08	0.13	0.14
	7	-	-	-	0.02	0.04	0
	8	-	-	-	-	0.05	0.04
	9	-	-	-	-	-	-0.1
NWMED SST	1	**2.19**	-	-	-	-	-
	2	**-1.86**	**3.05**	-	-	-	-
	3	-0.06	**-3.31**	**2.07**	-	-	-
	4	0.28	0.4	**-2.55**	**1.62**	-	-
	5	-	0.46	0.23	**-3.24**	**0.58**	-
	6	-	-	**0.67**	**2.23**	**-1.45**	-0.35
	7	-	-	-	-0.27	**1.84**	**0.98**
	8	-	-	-	-	**-0.71**	-0.23
	9	-	-	-	-	-	-0.26
CNAA SST	1	**-1.93**	-	-	-	-	-
	2	**2.22**	**-3.24**	-	-	-	-
	3	0.03	**3.67**	**-3.51**	-	-	-
	4	-0.3	0.47	**3.71**	**-5.09**	-	-
	5	-	**-1**	**1.8**	**10.26**	**-1.37**	-
	6	-	-	**-2.16**	**-7.29**	**3.49**	**1.38**
	7	-	-	-	**1.95**	**-4.52**	**-3.73**
	8	-	-	-	-	**2.24**	**3.05**
	9	-	-	-	-	-	**-0.76**

TABLE B1: **Regression coefficients for the MLR model** Coefficients with absolute values above 0.5 are bold.

Lead time		1 week		2 weeks		3 weeks		4 weeks		5 weeks		6 weeks	
Target		$+1\sigma$	$+1.5\sigma$	$+1\sigma$	$+1.5\sigma$	$+1\sigma$	$+1.5\sigma$	$+1\sigma$	$+1.5\sigma$	$+1\sigma$	$+1.5\sigma$	$+1\sigma$	$+1.5\sigma$
Predictor	**Lag (weeks)**												
Temperature	1	0.25	0.31	-	-	-	-	-	-	-	-	-	-
	2	-0.23	-0.24	-0.17	-0.15	-	-	-	-	-	-	-	-
	3	-0.05	-0.24	-0.23	-0.47	-0.17	-0.34	-	-	-	-	-	-
	4	-0.04	-0.07	-0.07	-0.08	-0.13	-0.21	-0.16	-0.25	-	-	-	-
	5	-	-	0.1	0.16	0.14	0.23	0.11	0.14	0.1	0.09	-	-
	6	-	-	-	-	0.08	0.06	0.12	0.22	0.11	0.22	0.12	0.2
	7	-	-	-	-	-	-	-0.03	-0.3	-0.02	-0.26	-0.02	-0.27
	8	-	-	-	-	-	-	-	-	-0.02	-0.05	0.06	0.05
	9	-	-	-	-	-	-	-	-	-	-	-0.16	-0.31
Geopotential	1	-0.04	-0.15	-	-	-	-	-	-	-	-	-	-
	2	0.17	0.27	0.15	0.24	-	-	-	-	-	-	-	-
	3	-0.02	0.16	0.14	0.37	0.09	0.28	-	-	-	-	-	-
	4	-0.03	-0.07	-0.01	-0.1	0.06	-0.03	0.05	0.01	-	-	-	-
	5	-	-	-0.1	-0.08	-0.12	-0.11	-0.09	-0.04	-0.13	-0.05	-	-
	6	-	-	-	-	-0.04	-0.09	-0.08	-0.22	-0.07	-0.19	-0.09	-0.16
	7	-	-	-	-	-	-	0.02	0.17	-0.03	0.07	-0.05	0.07
	8	-	-	-	-	-	-	-	-	0.08	0.14	0.05	0.11
	9	-	-	-	-	-	-	-	-	-	-	0.2	0.3
Precipitation	1	-0.3	-0.33	-	-	-	-	-	-	-	-	-	-
	2	0.04	-0.01	0.12	0.1	-	-	-	-	-	-	-	-
	3	0	0.04	0.06	0.13	0.04	0.13	-	-	-	-	-	-
	4	-0.04	0	-0.03	0	-0.01	0.02	-0.01	0.02	-	-	-	-
	5	-	-	-0.05	-0.05	-0.04	-0.05	-0.04	-0.01	-0.03	-0.03	-	-
	6	-	-	-	-	-0.05	-0.09	-0.03	-0.06	-0.01	-0.01	-0.03	-0.06
	7	-	-	-	-	-	-	0.03	-0.03	0.11	0.02	0.08	0
	8	-	-	-	-	-	-	-	-	0.11	0.07	0.12	0.1
	9	-	-	-	-	-	-	-	-	-	-	0.21	0.24
Soil moisture	1	0.46	0.47	-	-	-	-	-	-	-	-	-	-
	2	-0.32	-0.12	-0.07	0.11	-	-	-	-	-	-	-	-
	3	0.01	-0.16	-0.01	-0.22	-0.07	-0.14	-	-	-	-	-	-
	4	0.02	-0.09	0.09	-0.08	0.03	-0.17	-0.03	-0.26	-	-	-	-
	5	-	-	0	0.13	0.05	0.26	0.04	0.13	-0.03	-0.09	-	-
	6	-	-	-	-	0.03	-0.04	-0.02	0.11	-0.03	0.05	-0.02	0.04
	7	-	-	-	-	-	-	0.04	-0.06	-0.14	-0.17	-0.12	-0.14
	8	-	-	-	-	-	-	-	-	0.13	0.17	0.1	0.12
	9	-	-	-	-	-	-	-	-	-	-	-0.11	-0.14
SEA	1	-0.1	-0.13	-	-	-	-	-	-	-	-	-	-
	2	-0.02	-0.01	-0.04	-0.02	-	-	-	-	-	-	-	-
	3	-0.1	-0.14	-0.08	-0.1	-0.09	-0.12	-	-	-	-	-	-
	4	-0.1	-0.12	-0.1	-0.12	-0.1	-0.12	-0.1	-0.14	-	-	-	-
	5	-	-	0.08	0.15	0.07	0.15	0.08	0.16	0.06	0.12	-	-
	6	-	-	-	-	0.05	0.07	0.06	0.1	0.07	0.13	0.08	0.13
	7	-	-	-	-	-	-	0	-0.05	0.01	-0.04	-0.01	-0.07
	8	-	-	-	-	-	-	-	-	0.01	0.06	0.01	0.06
	9	-	-	-	-	-	-	-	-	-	-	-0.03	-0.1
NWMED SST	1	**0.98**	**1.17**	-	-	-	-	-	-	-	-	-	-
	2	**-1.07**	**-1.3**	**1.12**	**1.28**	-	-	-	-	-	-	-	-
	3	0.4	**0.62**	**-1.06**	**-1.31**	**0.71**	**0.82**	-	-	-	-	-	-
	4	-0.08	-0.27	0	0.22	**-0.68**	**-0.88**	**0.58**	**0.77**	-	-	-	-
	5	-	-	0.2	0.06	-0.29	0.01	**-0.98**	**-1.14**	0.26	0.25	-	-
	6	-	-	-	-	0.46	0.27	0.36	0.44	**-0.59**	-0.1	-0.04	0.45
	7	-	-	-	-	-	-	0.22	0.17	0.47	-0.31	0.13	**-0.53**
	8	-	-	-	-	-	-	-	-	-0.02	0.37	0	0.09
	9	-	-	-	-	-	-	-	-	-	-	0.01	0.18
CNAA SST	1	**-0.55**	-0.22	-	-	-	-	-	-	-	-	-	-
	2	**1.29**	**0.98**	**-0.73**	**-0.75**	-	-	-	-	-	-	-	-
	3	**-0.61**	**-0.82**	**0.86**	**0.66**	**-0.83**	**-1.22**	-	-	-	-	-	-
	4	-0.01	0.21	0.13	0.21	0.35	**0.79**	**-1.76**	**-2.29**	-	-	-	-
	5	-	-	-0.22	-0.13	**1.48**	**1.2**	**2.98**	**3.8**	**-0.85**	**-0.98**	-	-
	6	-	-	-	-	**-1.01**	**-0.83**	**-1.35**	**-2.04**	**1.58**	**1.1**	0.13	-0.39
	7	-	-	-	-	-	-	0.1	0.44	**-1**	-0.05	-0.4	0.44
	8	-	-	-	-	-	-	-	-	0.23	-0.19	**0.55**	0.28
	9	-	-	-	-	-	-	-	-	-	-	-0.27	-0.38

Table B2: **Regression coefficients for the RC$^+$ model** Coefficients with absolute values above 0.5 are bold. The regression coefficients for the RC$^-$ model are similar and are not shown here.

Lead time		1 week	2 weeks	3 weeks	4 weeks	5 weeks	6 weeks
Predictor	**Lag (weeks)**						
Temperature	1	0.02	-	-	-	-	-
	2	0.01	0.02	-	-	-	-
	3	0.01	0.01	0.01	-	-	-
	4	0.01	**0.05**	0.03	0.01	-	-
	5	-	0.01	0	0.01	0.01	-
	6	-	-	0.01	0.02	0.02	0.02
	7	-	-	-	0.03	0.03	0.01
	8	-	-	-	-	0.01	0.01
	9	-	-	-	-	-	0.01
Geopotential	1	**0.23**	-	-	-	-	-
	2	0.01	0	-	-	-	-
	3	0.01	0	0.01	-	-	-
	4	0.01	0.01	0.01	0	-	-
	5	-	0	0	0.01	0.01	-
	6	-	-	0	0.01	0.01	0
	7	-	-	-	0.02	0.02	0.01
	8	-	-	-	-	0.01	0
	9	-	-	-	-	-	0.01
Precipitation	1	**0.18**	-	-	-	-	-
	2	0.03	0.01	-	-	-	-
	3	0.01	0	0.01	-	-	-
	4	0	0	0	0.01	-	-
	5	-	0	0.01	0.01	0.01	-
	6	-	-	0.01	0.02	0.02	0.02
	7	-	-	-	0.01	0	0.01
	8	-	-	-	-	0.01	0
	9	-	-	-	-	-	0.02
Soil moisture	1	0.01	-	-	-	-	-
	2	0.01	0.02	-	-	-	-
	3	0.01	0.01	0.01	-	-	-
	4	0.02	0.01	0.02	0.02	-	-
	5	-	0.04	**0.05**	0.04	**0.05**	-
	6	-	-	**0.06**	**0.05**	**0.05**	**0.06**
	7	-	-	-	0.01	0.01	0.01
	8	-	-	-	-	0.02	0.03
	9	-	-	-	-	-	0.03
SEA	1	**0.07**	-	-	-	-	-
	2	0.01	0.03	-	-	-	-
	3	0.01	0.01	0.03	-	-	-
	4	0.01	0.01	0.01	0.02	-	-
	5	-	**0.06**	**0.07**	**0.06**	**0.05**	-
	6	-	-	0.04	0.02	0.02	0.04
	7	-	-	-	0.03	0.03	0.04
	8	-	-	-	-	0.01	0.01
	9	-	-	-	-	-	0.01
NWMED SST	1	**0.21**	-	-	-	-	-
	2	0.01	**0.39**	-	-	-	-
	3	0.03	0.04	**0.12**	-	-	-
	4	0.01	0.03	0.03	**0.07**	-	-
	5	-	0.01	**0.06**	0.04	**0.05**	-
	6	-	-	**0.08**	0.04	**0.05**	**0.05**
	7	-	-	-	**0.12**	**0.1**	**0.07**
	8	-	-	-	-	0.04	0.04
	9	-	-	-	-	-	**0.05**
CNAA SST	1	0.02	-	-	-	-	-
	2	0.02	**0.1**	-	-	-	-
	3	0.01	0.01	**0.13**	-	-	-
	4	0.02	0.03	0.03	**0.06**	-	-
	5	-	**0.09**	**0.06**	**0.1**	**0.13**	-
	6	-	-	**0.12**	**0.15**	**0.16**	**0.22**
	7	-	-	-	0.03	0.02	0.01
	8	-	-	-	-	**0.07**	0.03
	9	-	-	-	-	-	**0.16**

TABLE B3: **Predictor importances for the RFR model** Values above 0.04 are bold.

Lead time		**1 week**		**2 weeks**		**3 weeks**		**4 weeks**		**5 weeks**		**6 weeks**	
Target		***+1σ***	***+1.5σ***	***+1σ***	***+1.5σ***	***+1σ***	***+1.5σ***	***+1σ***	***+1.5σ***	***+1σ***	***+1.5σ***	***+1σ***	***+1.5σ***
Predictor	**Lag (weeks)**												
Temperature	1	**0.1**	**0.1**	-	-	-	-	-	-	-	-	-	-
	2	0.01	0.01	0.03	0.02	-	-	-	-	-	-	-	-
	3	0.02	0.03	0.02	0.02	0.02	0.01	-	-	-	-	-	-
	4	0.01	0.03	0.03	0.03	0.02	0.02	0.01	0.02	-	-	-	-
	5	-	-	0.03	0.02	0.02	0.02	0.02	0.02	0.01	0.02	-	-
	6	-	-	-	-	0.02	0.01	0.01	0.02	0.01	0.02	0.01	0.02
	7	-	-	-	-	-	-	0.02	0.04	0.01	0.04	0.01	0.04
	8	-	-	-	-	-	-	-	-	0.02	0.03	0.02	0.03
	9	-	-	-	-	-	-	-	-	-	-	0.02	0.03
Geopotential	1	**0.1**	**0.09**	-	-	-	-	-	-	-	-	-	-
	2	0.01	0.01	0.03	0.03	-	-	-	-	-	-	-	-
	3	0.01	0.01	0.02	0.02	0.02	0.02	-	-	-	-	-	-
	4	0.01	0.03	0.02	0.03	0.01	0.02	0.01	0.02	-	-	-	-
	5	-	-	0.03	0.03	0.01	0.01	0.01	0.02	0.01	0.02	-	-
	6	-	-	-	-	0.01	0.01	0.01	0.02	0.01	0.02	0.01	0.02
	7	-	-	-	-	-	-	0.03	0.03	0.02	0.03	0.02	0.03
	8	-	-	-	-	-	-	-	-	0.01	0.02	0.01	0.02
	9	-	-	-	-	-	-	-	-	-	-	0.01	0.02
Precipitation	1	**0.13**	**0.06**	-	-	-	-	-	-	-	-	-	-
	2	0.01	0.01	0.03	0.02	-	-	-	-	-	-	-	-
	3	0.01	0.02	0.02	0.02	0.01	0.02	-	-	-	-	-	-
	4	0.01	0.01	0.02	0.02	0.01	0.01	0.01	0.02	-	-	-	-
	5	-	-	0.03	0.02	0.01	0.01	0.01	0.02	0.01	0.02	-	-
	6	-	-	-	-	0.02	0.02	0.02	0.01	0.02	0.02	0.01	0.02
	7	-	-	-	-	-	-	0.01	0.02	0.01	0.02	0.02	0.02
	8	-	-	-	-	-	-	-	-	0.01	0.03	0.02	0.03
	9	-	-	-	-	-	-	-	-	-	-	**0.05**	0.04
Soil moisture	1	0.03	0.03	-	-	-	-	-	-	-	-	-	-
	2	0.02	0.02	0.03	0.04	-	-	-	-	-	-	-	-
	3	0.01	0.01	0.03	0.03	0.01	0.02	-	-	-	-	-	-
	4	0.01	0.02	0.03	0.03	0.02	0.02	0.02	0.03	-	-	-	-
	5	-	-	0.04	0.04	0.03	**0.06**	0.03	**0.06**	0.03	**0.05**	-	-
	6	-	-	-	-	0.03	0.03	0.04	0.03	0.04	0.03	0.04	0.04
	7	-	-	-	-	-	-	0.03	0.03	0.01	0.03	0.02	0.04
	8	-	-	-	-	-	-	-	-	0.04	0.02	**0.05**	0.03
	9	-	-	-	-	-	-	-	-	-	-	0.02	0.03
SEA	1	**0.09**	**0.07**	-	-	-	-	-	-	-	-	-	-
	2	0.02	0.02	0.04	0.04	-	-	-	-	-	-	-	-
	3	0.03	0.03	0.04	**0.05**	**0.07**	**0.08**	-	-	-	-	-	-
	4	0.02	0.02	0.04	0.03	0.04	0.03	**0.05**	0.04	-	-	-	-
	5	-	-	0.04	**0.05**	0.03	0.03	0.03	0.04	0.04	0.04	-	-
	6	-	-	-	-	0.03	0.03	0.03	0.03	0.03	0.03	0.03	0.03
	7	-	-	-	-	-	-	0.02	0.02	0.02	0.02	0.03	0.02
	8	-	-	-	-	-	-	-	-	0.01	0.03	0.02	0.02
	9	-	-	-	-	-	-	-	-	-	-	0.02	0.04
NWMED SST	1	**0.09**	**0.13**	-	-	-	-	-	-	-	-	-	-
	2	**0.05**	0.04	**0.08**	**0.08**	-	-	-	-	-	-	-	-
	3	0.03	0.03	**0.06**	**0.06**	**0.08**	**0.09**	-	-	-	-	-	-
	4	0.02	0.02	0.04	0.04	**0.05**	**0.06**	**0.05**	0.04	-	-	-	-
	5	-	-	0.04	0.04	**0.06**	**0.06**	**0.06**	0.04	0.03	**0.05**	-	-
	6	-	-	-	-	**0.05**	**0.07**	**0.07**	**0.06**	**0.07**	**0.05**	**0.06**	**0.05**
	7	-	-	-	-	-	-	0.04	**0.05**	**0.07**	**0.05**	0.04	**0.05**
	8	-	-	-	-	-	-	-	-	0.04	0.04	**0.06**	0.04
	9	-	-	-	-	-	-	-	-	-	-	**0.06**	**0.06**
CNAA SST	1	0.03	0.03	-	-	-	-	-	-	-	-	-	-
	2	0.04	0.03	**0.06**	**0.05**	-	-	-	-	-	-	-	-
	3	0.03	0.02	**0.05**	0.04	**0.06**	0.04	-	-	-	-	-	-
	4	0.04	0.02	0.04	0.04	**0.07**	0.04	**0.06**	0.04	-	-	-	-
	5	-	-	**0.06**	**0.06**	**0.09**	**0.07**	**0.13**	**0.07**	**0.12**	**0.06**	-	-
	6	-	-	-	-	**0.1**	**0.09**	**0.11**	**0.06**	**0.16**	**0.07**	**0.12**	**0.06**
	7	-	-	-	-	-	-	**0.07**	**0.08**	**0.08**	**0.06**	**0.09**	**0.06**
	8	-	-	-	-	-	-	-	-	**0.07**	**0.06**	**0.09**	**0.05**
	9	-	-	-	-	-	-	-	-	-	-	**0.05**	**0.06**

TABLE B4: **Predictor importances for the RFC^{+} model** Values above 0.04 are bold. The importances for the RFC^{-} model are similar and are not shown here. However, for the *+1*σ heatwave index, the RFC^{-} model relies more strongly on the *soil moisture* and on the *SEA* at long lead times (3–6 weeks) than the RFC^{+} model does.

APPENDIX C

Regression forecasts

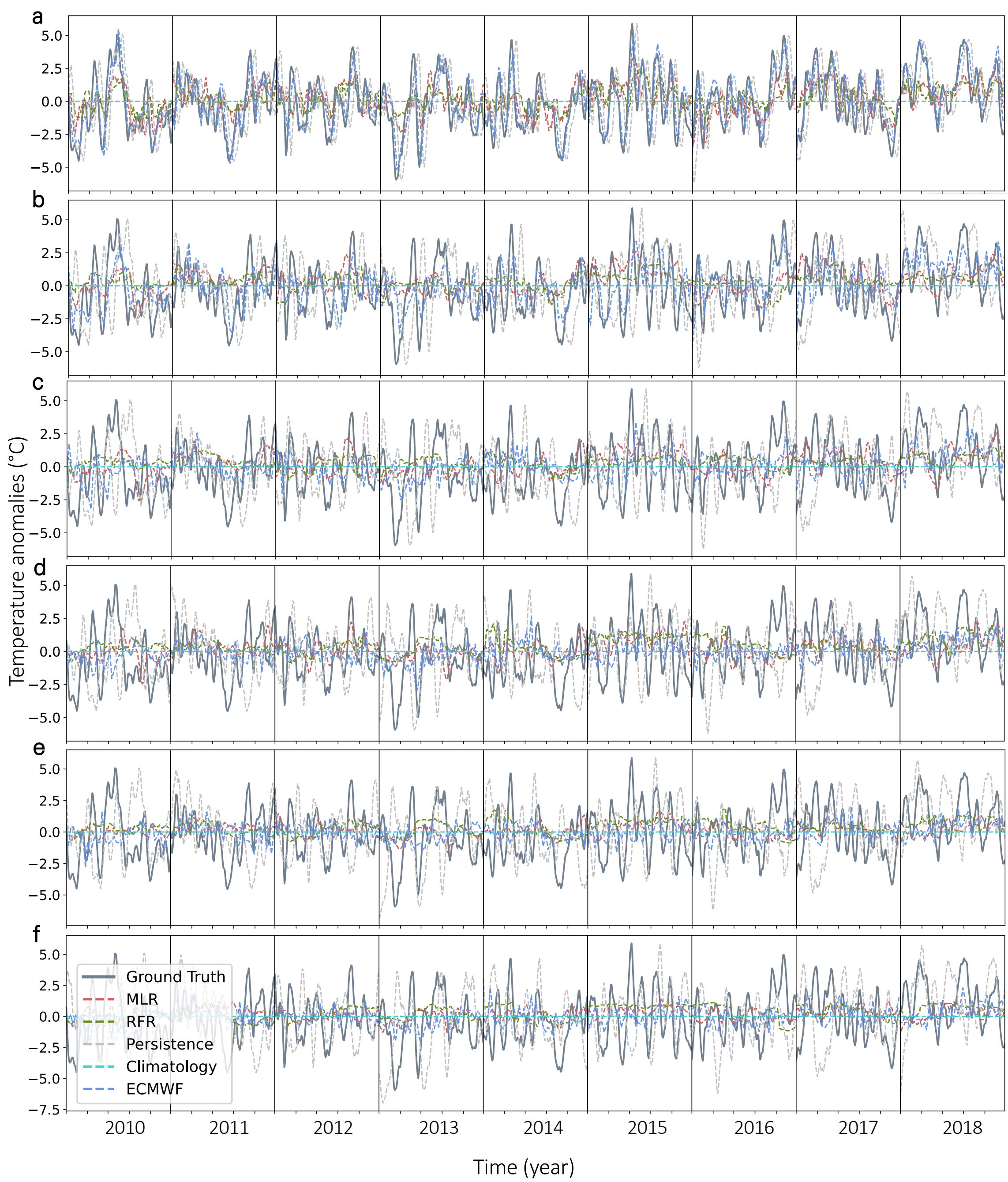

Fig. C1: **Regression time series** The ground truth time series, the reference forecasts, and the predictions by the ML regression models of the temperature anomalies are shown for the nine summers in the test time period (2010–2018). Sub-figures a–f correspond to lead times 1–6, respectively.

References

Barriopedro, D., E. M. Fischer, J. Luterbacher, R. M. Trigo, and R. Garcia-Herrera, 2011: The hot summer of 2010: Redrawing the temperature record map of europe. *Science*, **332**, 220–224, https://doi.org/10.1126/science.1201224.

Bassil, K., and D. Cole, 2010: Effectiveness of public health interventions in reducing morbidity and mortality during heat episodes: a structured review. *International Journal of Environmental Research and Public Health*, **7**, 991–1001, https://doi.org/10.3390/ijerph7030991.

Basu, R., 2002: Relation between elevated ambient temperature and mortality: a review of the epidemiologic evidence. *Epidemiologic Reviews*, **24**, 190–202, https://doi.org/10.1093/epirev/mxf007.

Black, E., M. Blackburn, G. Harrison, B. Hoskins, and J. Methven, 2004: Factors contributing to the summer 2003 european heatwave. *Weather*, **59**, 217–223, https://doi.org/10.1256/wea.74.04.

Bladé, I., B. Liebmann, D. Fortuny, and G. J. van Oldenborgh, 2011: Observed and simulated impacts of the summer nao in europe: Implications for projected drying in the mediterranean region. *Climate Dynamics*, **39**, 709–727, https://doi.org/10.1007/s00382-011-1195-x.

Bradley, A. P., 1997: The use of the area under the roc curve in the evaluation of machine learning algorithms. *Pattern Recognition*, **30**, 1145–1159, https://doi.org/10.1016/s0031-3203(96)00142-2.

Brownlee, J., 2020: A gentle introduction to threshold-moving for imbalanced classification. URL https://machinelearningmastery.com/threshold-moving-for-imbalanced-classification/.

Brownlee, J., 2021: *Imbalanced Classification with Python: Choose Better Metrics, Balance Skewed Classes, and Apply Cost-sensitive Learning*. v1.3 ed., Ebook, 246–260 pp., URL https://machinelearningmastery.com/imbalanced-classification-with-python/.

Chattopadhyay, A., E. Nabizadeh, and P. Hassanzadeh, 2020: Analog forecasting of extreme-causing weather patterns using deep learning. *Journal of Advances in Modeling Earth Systems*, **12**, 1942–2466, https://doi.org/10.1029/2019ms001958.

Cho, D., C. Yoo, J. Im, and D. Cha, 2020: Comparative assessment of various machine learning-based bias correction methods for numerical weather prediction model forecasts of extreme air temperatures in urban areas. *Earth and Space Science*, **7**, 2333–5084, https://doi.org/10.1029/2019ea000740.

Cornes, R. C., G. van der Schrier, E. J. M. van den Besselaar, and P. D. Jones, 2018: An ensemble version of the e-obs temperature and precipitation data sets. *Journal of Geophysical Research: Atmospheres*, **123**, 9391–9409, https://doi.org/10.1029/2017jd028200.

de Perez, E. C., and Coauthors, 2018: Global predictability of temperature extremes. *Environmental Research Letters*, **13**, 1748–9318, https://doi.org/10.1088/1748-9326/aab94a.

Deb, P., H. Moradkhani, P. Abbaszadeh, A. S. Kiem, J. Engström, D. Keellings, and A. Sharma, 2020: Causes of the widespread 2019–2020 australian bushfire season. *Earth's Future*, **8**, 2328–4277, https://doi.org/10.1029/2020ef001671.

Dee, D. P., and Coauthors, 2011: The era-interim reanalysis: configuration and performance of the data assimilation system. *Quarterly Journal of the Royal Meteorological Society*, **137**, 553–597, https://doi.org/10.1002/qj.828.

Dong, B., R. T. Sutton, T. Woollings, and K. Hodges, 2013: Variability of the north atlantic summer storm track: Mechanisms and impacts on european climate. *Environmental Research Letters*, **8**, https://doi.org/10.1088/1748-9326/8/3/034037.

Duchez, A., and Coauthors, 2016: Drivers of exceptionally cold north atlantic ocean temperatures and their link to the 2015 european heat wave. *Environmental Research Letters*, **11**, https://doi.org/10.1088/1748-9326/11/7/074004.

Fischer, E. M., S. I. Seneviratne, P. L. Vidale, D. Lüthi, and C. Schär, 2007: Soil moisture–atmosphere interactions during the 2003 european summer heat wave. *J. Climate*, **20**, 5081–5099, https://doi.org/10.1175/jcli4288.1.

Ford, T. W., P. A. Dirmeyer, and D. O. Benson, 2018: Evaluation of heat wave forecasts seamlessly across subseasonal timescales. *Npj Climate and Atmospheric Science*, **1**, https://doi.org/10.1038/s41612-018-0027-7.

Haiden, T., M. Janousek, F. Vitart, Z. B. Bouallegue, L. Ferranti, F. Prates, and D. Richardson, 2019: Technical memorandum: Evaluation of ecmwf forecasts, including the 2019 upgrade. 10.21957/mlvapkke, URL https://www.ecmwf.int/node/19277.

Kautz, L.-A., O. Martius, S. Pfahl, J. G. Pinto, A. M. Ramos, P. M. Sousa, and T. Woollings, 2022: Atmospheric blocking and weather extremes over the euro-atlantic sector – a review. *Weather and Climate Dynamics*, **3**, 305–336, https://doi.org/10.5194/wcd-3-305-2022.

Khan, N., S. Shahid, L. Juneng, K. Ahmed, T. Ismail, and N. Nawaz, 2019: Prediction of heat waves in pakistan using quantile regression forests. *Atmospheric Research*, **221**, 1–11, https://doi.org/10.1016/j.atmosres.2019.01.024.

Kolstad, E. W., E. A. Barnes, and S. P. Sobolowski, 2017: Quantifying the role of land-atmosphere feedbacks in mediating near-surface temperature persistence. *Quarterly Journal of the Royal Meteorological Society*, **143**, 1620–1631, https://doi.org/10.1002/qj.3033.

Kretschmer, M., J. Runge, and D. Coumou, 2017: Early prediction of extreme stratospheric polar vortex states based on causal precursors. *Geophysical Research Letters*, **44**, 8592–8600, https://doi.org/10.1002/2017gl074696.

Kämäräinen, M., P. Uotila, A. Y. Karpechko, O. Hyvärinen, I. Lehtonen, and J. Räisänen, 2019: Statistical learning methods as a basis for skillful seasonal temperature forecasts in europe. *J. Climate*, **32**, 5363–5379, https://doi.org/10.1175/jcli-d-18-0765.1.

Lehmann, J., M. Kretschmer, B. Schauberger, and F. Wechsung, 2020: Potential for early forecast of moroccan wheat yields based on climatic drivers. *Geophysical Research Letters*, **47**, 94–8276, https://doi.org/10.1029/2020gl087516.

Lemaitre, G., F. Nogueira, and C. K. Aridas, 2017: Imbalanced-learn: a python toolbox to tackle the curse of imbalanced datasets in machine learning. *Journal of Machine Learning Research*, **18**, 1–5.

Li, M., Y. Yao, I. Simmonds, D. Luo, L. Zhong, and X. Chen, 2020: Collaborative impact of the nao and atmospheric blocking on european heatwaves, with a focus on the hot summer of 2018. *Environmental Research Letters*, **15**, https://doi.org/10.1088/1748-9326/aba6ad.

Liu, Y., and Coauthors, 2016: Application of deep convolutional neural networks for detecting extreme weather in climate datasets. *arXiv*, https://doi.org/10.48550/ARXIV.1605.01156.

Loughnan, M., 2014: Heatwaves are silent killers. *Geodate*, **37**, 1–10.

Lowe, D., K. L. Ebi, and B. Forsberg, 2011: Heatwave early warning systems and adaptation advice to reduce human health consequences of heatwaves. *International Journal of Environmental Research and Public Health*, **8**, 4623–4648, https://doi.org/10.3390/ijerph8124623.

Mecking, J. V., S. S. Drijfhout, J. J.-M. Hirschi, and A. T. Blaker, 2019: Ocean and atmosphere influence on the 2015 european heatwave. *Environmental Research Letters*, **14**, https://doi.org/10.1088/1748-9326/ab4d33.

Mehta, P., M. Bukov, C.-H. Wang, A. G. Day, C. Richardson, C. K. Fisher, and D. J. Schwab, 2019: A high-bias, low-variance introduction to machine learning for physicists. *Physics Reports*, **810**, 1–124, https://doi.org/10.1016/j.physrep.2019.03.001.

Merz, B., and Coauthors, 2020: Impact forecasting to support emergency management of natural hazards. *Reviews of Geophysics*, **58**, 8755–1209, https://doi.org/10.1029/2020rg000704.

Mishra, M., 2018: Regularization: an important concept in machine learning. URL https://towardsdatascience.com/regularization-an-important-concept-in-machine-learning-5891628907ea.

Murphy, A. H., 1993: What is a good forecast? an essay on the nature of goodness in weather forecasting. *Wea. Forecasting*, **8**, 281–293, https://doi.org/10.1175/1520-0434(1993)008<0281:wiagfa>2.0.co;2.

Muñoz-Sabater, J., and Coauthors, 2021: Era5-land: a state-of-the-art global reanalysis dataset for land applications. *Earth System Science Data*, **13**, 4349–4383, https://doi.org/10.5194/essd-13-4349-2021.

Oliveira, J. C., E. Zorita, V. Koul, T. Ludwig, and J. Baehr, 2020: Forecast opportunities for european summer climate ensemble predictions using self-organising maps. *Proceedings of the 10th International Conference on Climate Informatics*, 67–71, https://doi.org/10.1145/3429309.3429319.

Ossó, A., R. Sutton, L. Shaffrey, and B. Dong, 2020: Development, amplification, and decay of atlantic/european summer weather patterns linked to spring north atlantic sea surface temperatures. *J. Climate*, **33**, 5939–5951, https://doi.org/10.1175/JCLI-D-19-0613.1.

Pedregosa, F., and Coauthors, 2011: Scikit-learn: Machine learning in python. *Journal of Machine Learning Research*, **12**, 2825–2830.

Perkins, S. E., 2015: A review on the scientific understanding of heatwaves -their measurement, driving mechanisms, and changes at the global scale. *Atmospheric Research*, **164–165**, 242–267, https://doi.org/10.1016/j.atmosres.2015.05.014.

Perkins, S. E., and L. V. Alexander, 2013: On the measurement of heat waves. *J. Climate*, **26**, 4500–4517, https://doi.org/10.1175/jcli-d-12-00383.1.

Perkins-Kirkpatrick, S. E., and S. C. Lewis, 2020: Increasing trends in regional heatwaves. *Nature Communications*, **11**, https://doi.org/10.1038/s41467-020-16970-7.

Poli, P., and Coauthors, 2016: Era-20c: An atmospheric reanalysis of the twentieth century. *J. Climate*, **29**, 4083–4097, https://doi.org/10.1175/jcli-d-15-0556.1.

Pyrina, M., M. Nonnenmacher, S. Wagner, and E. Zorita, 2021: Statistical seasonal prediction of european summer mean temperature using observational, reanalysis and satellite data. *Weather and Forecasting*, **36**, https://doi.org/10.1175/waf-d-20-0235.1.

Racah, E., C. Beckham, T. Maharaj, S. E. Kahou, Prabhat, and C. Pal, 2016: Extremeweather: A large-scale climate dataset for semi-supervised detection, localization, and understanding of extreme weather events. *arXiv*, https://doi.org/10.48550/ARXIV.1612.02095.

Rasp, S., and N. Thuerey, 2021: Data-driven medium-range weather prediction with a resnet pretrained on climate simulations: A new model for weatherbench. *Journal of Advances in Modeling Earth Systems*, **13**, 1942–2466, https://doi.org/10.1029/2020ms002405.

Rayner, N. A., D. E. Parker, E. B. Horton, C. K. Folland, L. V. Alexander, D. P. Rowell, E. C. Kent, and A. Kaplan, 2003: Global analyses of sea surface temperature, sea ice, and night marine air temperature since the late nineteenth century. *Journal of Geophysical Research*, **108**, 148–227, https://doi.org/10.1029/2002jd002670.

Reichstein, M., G. Camps-Valls, B. Stevens, M. Jung, J. Denzler, and N. Carvalhais, 2019: Deep learning and process understanding for data-driven earth system science. *Nature*, **566**, 195–204, https://doi.org/10.1038/s41586-019-0912-1.

Robertson, A. W., A. Kumar, M. Peña, and F. Vitart, 2015: Improving and promoting subseasonal to seasonal prediction. *Bull. Amer. Meteor. Soc.*, **96**, ES49–ES53, https://doi.org/10.1175/bams-d-14-00139.1.

Rudin, C., 2019: Stop explaining black box machine learning models for high stakes decisions and use interpretable models instead. *Nature Machine Intelligence*, **1**, 206–215, https://doi.org/10.1038/s42256-019-0048-x.

Seneviratne, S. I., T. Corti, E. L. Davin, M. Hirschi, E. B. Jaeger, I. Lehner, B. Orlowsky, and A. J. Teuling, 2010: Investigating soil moisture–climate interactions in a changing climate: a review. *Earth-Science Reviews*, **99**, 125–161, https://doi.org/10.1016/j.earscirev.2010.02.004.

Seneviratne, S. I., M. G. Donat, B. Mueller, and L. V. Alexander, 2014: No pause in the increase of hot temperature extremes. *Nature Climate Change*, **4**, 161–163, https://doi.org/10.1038/nclimate2145.

Sobhani, N., D. del Vento, and A. Fanfarillo, 2018: Long-lead forecast of heatwaves in the eastern united states using artificial intelligence. *Proceedings of the Amer. Geophysical Union, Fall Meeting 2018*.

Spensberger, C., and Coauthors, 2020: Dynamics of concurrent and sequential central european and scandinavian heatwaves. *Quarterly Journal of the Royal Meteorological Society*, **146**, 2998–3013, https://doi.org/10.1002/qj.3822.

Storch, H. V., and F. W. Zwiers, 2003: *Statistical analysis in climate research*. Cambridge University Press, 293–299 pp.

Suarez-Gutierrez, L., W. A. Mueller, C. Li, and J. Marotzke, 2020: Dynamical and thermodynamical drivers of variability in european summer heat extremes. *Climate Dynamics*, **54**, 4351–4366, https://doi.org/10.1007/s00382-020-05233-2.

Swets, J. A., R. M. Dawes, and J. Monahan, 2000: Psychological science can improve diagnostic decisions. *Psychological Science in the Public Interest*, **1**, 1–26, https://doi.org/10.1111/1529-1006.001.

US EPA, O., 2016: Climate change indicators: Heat-related deaths. URL https://www.epa.gov/climate-indicators/climate-change-indicators-heat-related-deaths.

Vabalas, A., E. Gowen, E. Poliakoff, and A. J. Casson, 2019: Machine learning algorithm validation with a limited sample size. *PLOS ONE*, **14**, https://doi.org/10.1371/journal.pone.0224365.

van Straaten, C., K. Whan, D. Coumou, B. van den Hurk, and M. Schmeits, 2022: Using explainable machine learning forecasts to discover sub-seasonal drivers of high summer temperatures in western and central europe. *Mon. Wea. Rev.*, https://doi.org/10.1175/mwr-d-21-0201.1.

Vijverberg, S., M. Schmeits, K. van der Wiel, and D. Coumou, 2020: Subseasonal statistical forecasts of eastern u.s. hot temperature events. *Mon. Wea. Rev.*, **148**, 4799–4822, https://doi.org/10.1175/mwr-d-19-0409.1.

Wallemacq, P., R. Below, and D. McClean, 2018: Economic losses, poverty and disasters (1998–2017). URL https://www.undrr.org/publication/economic-losses-poverty-disasters-1998-2017, 1–9 pp.

White, C. J., and Coauthors, 2017: Potential applications of subseasonal-to-seasonal (s2s) predictions. *Meteorological Applications*, **24**, 315–325, https://doi.org/10.1002/met.1654.

White, C. J., and Coauthors, 2021: Advances in the application and utility of subseasonal-to-seasonal predictions. *Bull. Amer. Meteor. Soc.*, **aop**, 1–57, https://doi.org/10.1175/bams-d-20-0224.1.

WMO, 2021: Climate adaptation summit: Invest in early warnings and early action. URL https://public.wmo.int/en/media/press-release/climate-adaptation-summit-invest-early-warnings-and-early-action.

Wulff, C. O., R. J. Greatbatch, D. I. V. Domeisen, G. Gollan, and F. Hansen, 2017: Tropical forcing of the summer east atlantic pattern. *Geophysical Research Letters*, **44**, 94–8276, https://doi.org/10.1002/2017gl075493.

Yiu, T., 2019: Understanding random forest. Towards Data Science, URL https://towardsdatascience.com/understanding-random-forest-58381e0602d2.

Zschenderlein, P., S. Pfahl, H. Wernli, and A. H. Fink, 2020: A lagrangian analysis of upper-tropospheric anticyclones associated with heat waves in europe. *Weather and Climate Dynamics*, **1**, 191–206, https://doi.org/10.5194/wcd-1-191-2020.